Geochemistry Geophysics Geosystems G3

Article
Volume 12, Number 7
1 July 2011
Q07001, doi:10.1029/2011GC003611
ISSN: 1525-2027

Published by AGU and the Geochemical Society

Imaging crustal and upper mantle structure beneath the Colorado Plateau using finite frequency Rayleigh wave tomography

Kaijian Liu
Department of Earth Science, Rice University, Houston, Texas 77005, USA (lkjcammit@gmail.com)

Applied Physics Program, Rice University, Houston, Texas 77005, USA

Alan Levander and Fenglin Niu
Department of Earth Science, Rice University, Houston, Texas 77005, USA

Meghan S. Miller
Department of Earth Sciences, University of Southern California, California 90089, USA

[1] A new 3-D shear velocity model of the crust and upper mantle beneath the Colorado Plateau and surrounding regions of the southwestern United States was made with finite frequency Rayleigh wave tomography using EarthScope/USArray data. The goal of our study is to examine the Colorado Plateau lithospheric modification that has resulted from Cenozoic tectonism and magmatism. We have inverted for the isotropic Vs model from a grid of Rayleigh wave dispersion curves obtained by a modified two-plane wave method for periods from 20 to 167 s. We map the lithosphere-asthenosphere boundary under the Colorado Plateau by identifying the middle of the shallowest upper mantle negative Vs gradient. The depths of the lithosphere-asthenosphere boundary inferred here agree well with receiver function estimates made independently. The strong lateral heterogeneity of shear velocity can be mainly attributed to 200–400 K variations in temperature together with ~1% partial melt fraction in the shallow upper mantle. The resulting Vs structures clearly image the upper mantle low-velocity zones under the Colorado Plateau margins that are associated with magmatic encroachment. These upper mantle low-velocity zones resulted from the convective removal of the Colorado Plateau lithosphere that had been rehydrated by subduction-released water, refertilizing and destabilizing it. This convective erosion by the asthenosphere at the low-viscosity part of the lithosphere is driven by the large step in lithospheric thickness and the thermal gradient across the boundary between the plateau and the extended Basin and Range since the Mid-Cenozoic at a rate similar to that of magmatic migration into the plateau from the southeast, south, and northwest. Moreover, the Rayleigh wave tomography model images parts of a high-velocity drip in the western Colorado Plateau and thus provides additional seismic evidence for ongoing convective downwelling of the lithosphere that was initially suggested by receiver functions and body wave tomography. The widespread edge convective erosion, which the regional delamination-style downwelling processes are a 3-D manifestation of, could provide additional buoyancy sources to support the excess uplift at the margins of the plateau.

Components: 12,000 words, 12 figures.

Keywords: Colorado Plateau; Rayleigh wave tomography; lithospheric delamination; partial melt; small-scale convection.

Index Terms: 7218 Seismology: Lithosphere (1236); 7255 Seismology: Surface waves and free oscillations; 8180 Tectonophysics: Tomography (6982, 7270).

Received 15 March 2011; **Accepted** 16 May 2011; **Published** 1 July 2011.

Liu, K., A. Levander, F. Niu, and M. S. Miller (2011), Imaging crustal and upper mantle structure beneath the Colorado Plateau using finite frequency Rayleigh wave tomography, *Geochem. Geophys. Geosyst.*, *12*, Q07001, doi:10.1029/2011GC003611.

1. Introduction

[2] In this paper we describe analysis and interpretation of fundamental mode Rayleigh waves across the Colorado Plateau (CP) and across its borders with the surrounding provinces using finite frequency Rayleigh wave tomography. The CP is a high-standing (~1.8–2.0 km), relatively stable physiographic province in the tectonically active southwestern United States (Figure 1). This distinct province is bounded by the Uinta Mountains and the Wasatch front in the north, the highly deformed Southern Rocky Mountains (SRM) in the northeast, the Rio Grande Rift (RGR) valley in the east, and the highly extended Basin and Range Province (BRP) in the south, west and southwest. Between the Southern Basin and Range (SBR) and the plateau, there is a ~100 km broad zone with transitional geologic and geophysical characteristics including normal faulting and recent magmatism (the CP-BR transition region). The Colorado Mineral Belt and the Jemez lineament are two distinct geologic features [*Humphreys et al.*, 2003] lying at the CP-SRM and CP-RGR boundaries, respectively (Figure 1). The availability of the Transportable Array data from the EarthScope/USArray project provides an unparalleled opportunity to construct high-resolution tomographic images in the tectonically active southwestern United States. Prior to the EarthScope/USArray program, seismic investigation of the CP and its adjacent regions was limited to either regional and continental-scale tomography studies, with rather poorly sampled data [e.g., *Humphreys and Dueker*, 1994; *van der Lee and Nolet*, 1997], or only relatively small regions or active source seismic profiles [e.g., *McCarthy et al.*, 1991; *McCarthy and Parsons*, 1994; *Wolf and Cipar*, 1993; *Parsons et al.*, 1996; *Sheehan et al.*, 1995, 1997; *Zandt et al.*, 1995; *Henstock et al.*, 1998; *Snelson et al.*, 1998, 2005; *Levander et al.*, 2005; *Wilson et al.*, 2005a, 2005b, 2010]. Since USArray, additional studies have provided new velocity models for the uppermost [*Buehler and Shearer*, 2010] and upper mantle [e.g., *Schmandt and Humphreys*, 2010] beneath the Colorado Plateau region, as well as Moho and LAB depth [*Miller and Levander*, 2009]. Our Rayleigh wave tomography using USArray can provide better vertical resolution in the upper mantle above ~200 km with absolute shear velocity information, complementing the body wave tomography, which provides relative velocity perturbations.

1.1. Tectonic History

[3] The modern lithospheric structures beneath the CP and its adjacent provinces in the southwestern United States are complicated mainly due to significant Cenozoic modifications to a Paleozoic passive continental margin outboard of a Proterozoic and Archean core [e.g., *Lipman*, 1992; *Lee et al.*, 2001; *Humphreys et al.*, 2003]. The NE striking continental lithosphere was assembled in the Proterozoic through progressive accretion of island arc terranes [*Karlstrom and Humphreys*, 1998]. The major lithospheric modification of the Paleozoic passive continental margin to the cratonic edge resulted from shortening, extension and magmatism in the western United States associated with Late Cretaceous-Early Cenozoic Farallon plate subduction beneath the North American plate [e.g., *Coney and Reynolds*, 1977; *Humphreys et al.*, 2003]. The rapid slab subduction initiated basement-cored uplift due to crustal compression/thickening during the Laramide orogeny (~70–45 Ma), and an eastward migration of arc magmatism [*Coney and Reynolds*, 1977; *Snyder et al.*, 1976] many hundred kilometers inland from the trench. As the Farallon slab began to flatten due to the combined effects of oceanic subduction and enhanced mantle wedge suction [*Humphreys*, 2009], it subsequently hydrated the base of the North American lithosphere [*Saleeby*, 2003; *Humphreys et al.*, 2003; *English et al.*, 2003], depressing the peridotite solidus for subsequent melting [*Lee*, 2005]. Following the slab removal ~30 Ma, Mid-Tertiary Basin and Range volcanism and extension are thought to have been triggered by postsubduction orogenic collapse as well as the exposure of the mantle lithosphere to hot ascending asthenosphere [*Dickinson and Snyder*, 1978; *Humphreys*, 1995]. Small-scale convection under the back arc and orogenic belt [*Wilson et al.*, 2005a, 2005b; *West et al.*, 2004; *Hyndman et al.*, 2005; *Humphreys*, 2009], along with dynamic mantle upwelling [*Moucha et al.*, 2008, 2009; *Liu et al.*, 2010], further modified the unstable southwestern U.S. lithosphere after the slab began foundering. Magmatism and extension continue presently in the BRP and RGR and are migrating

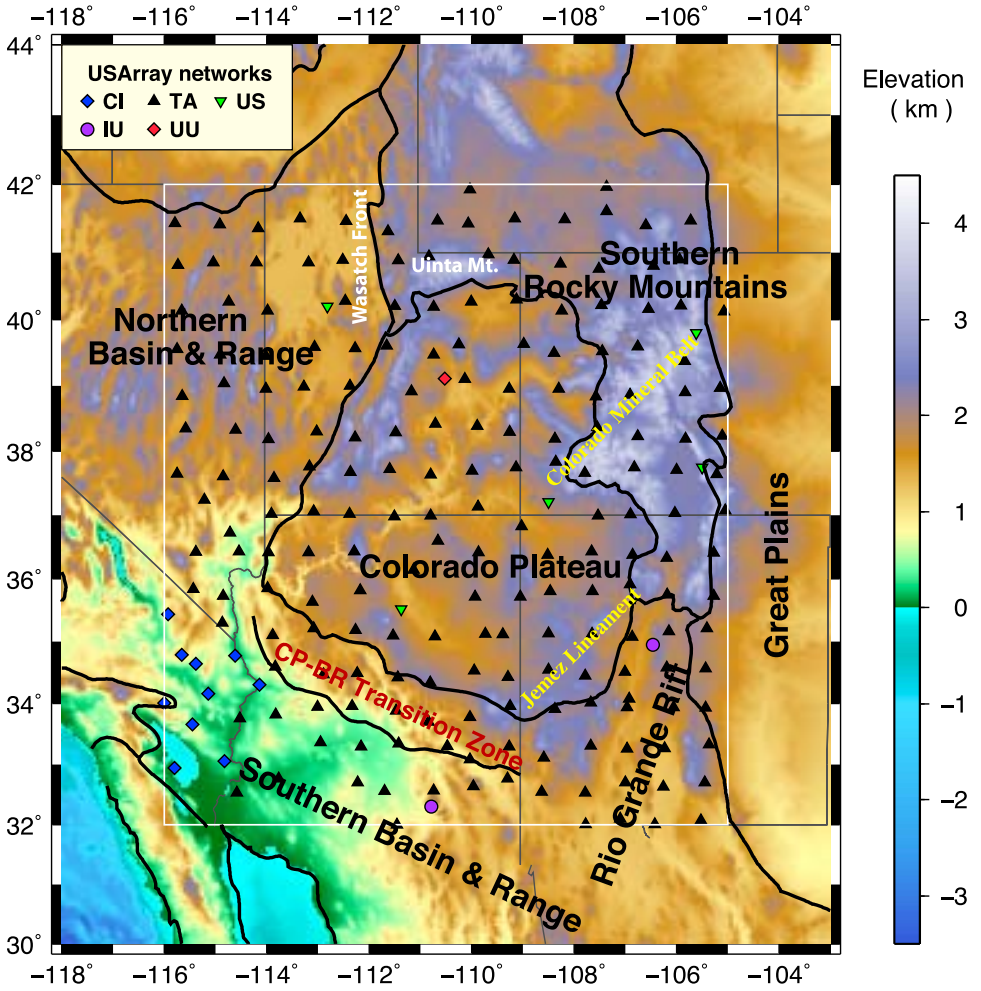

Figure 1. Topography map of the major physiographic provinces of the southwestern United States, including the Colorado Plateau, the southern and northern Basin and Range, the Rio Grande Rift, the Southern Rocky Mountains, and the Great Plains. Station distribution inside the study area (white box) from various USArray networks (TA, Transportable Array; CI, Caltech Regional Seismic; U.S., U.S. National Seismic; IU, IRIS/USGS; UU, University of Utah Regional) are also shown with different symbols (see legend). The topography data are from the ETOPO1 model (http://www.ngdc.noaa.gov/mgg/global/global.html) [*Amante and Eakins*, 2009]. Locations of the Colorado Mineral Belt and the NE trending Jemez lineament are also indicated.

into the CP margins at rates of ~3–6 km/Ma [*Roy et al.*, 2009]. During the past 30 Ma, the RGR has undergone a two-stage rifting process separated by a ~10 Ma period of magmatic quiescence [e.g., *Morgan et al.*, 1986]. It is still unclear how deformation and magmatism have altered the North American lithosphere beneath the CP and the neighboring provinces [*Humphreys*, 2009].

1.2. Motivation

[4] Small-scale convection such as edge-driven convection [e.g., *van Wijk et al.*, 2008, 2010] or convective destabilization of the Proterozoic lithospheric core beneath the CP [*Humphreys et al.*, 2003; *Levander et al.*, 2011] has been suggested to explain the unusually large velocity contrast across the transition edges. Based on the 2-D seismic tomography from the La RISTRA experiment [e.g., *West et al.*, 2004; *Gao et al.*, 2004; *Sine et al.*, 2008] and geodynamic modeling, *van Wijk et al.* [2010] suggested that edge-driven convection caused the Late Cenozoic magmatism and uplift at the edges between the CP and BRP or RGR. Whether such convective erosion at the CP margins is a localized or widespread feature remains unclear, and our Rayleigh wave tomographic image pro-

vides a comprehensive seismic model to examine the convective erosion around the transition area into the center of the plateau. Moreover, our model provides an independent study to understand the complicated physical state under the western CP. Complex Ps conversions beneath much of the plateau have been noted in receiver function (RF) studies [*McCarthy and Parsons*, 1994; *Zandt et al.*, 1995; *Sheehan et al.*, 1997; *Wilson et al.*, 2005a; *Gilbert et al.*, 2007; *Miller and Levander*, 2009]. *Gilbert and Sheehan* [2004] suggested that the weak Ps conversion might be introduced by a gradational impedance transition possibly caused by magmatic underplating [*Wolf and Cipar*, 1993]. However, *Levander et al.* [2011] proposed a delamination-style lithospheric downwelling under the western margin of the CP to explain the split of Moho signals observed in the receiver function volume using USArray data. Most of the converted amplitudes beneath the western plateau separate into discrete positive events with weak amplitudes compared to those of the surrounding tectonic regions. A high-resolution Vs model can improve our understanding of the regional lithosphere-asthenosphere interaction, as well as the complicated lithospheric convection beneath the western CP.

[5] A detailed 3-D Vs model can also help to understand the CP uplift mechanism, which remains the subject of a long-standing debate. Numerous mechanisms have been suggested to explain the ~2 km Cenozoic rock/surface uplift of the plateau since 80 Ma. The buoyancy sources from the crust, mantle lithosphere and asthenosphere can mainly be attributed to four major factors: thermal expansion [*Thompson and Zoback*, 1979; *Roy et al.*, 2009], mechanical lithospheric thinning [*Bird*, 1979; *Spencer*, 1996; *Lastowka et al.*, 2001], crustal thickening [*Morgan and Swanberg*, 1985; *McQuarrie and Chase*, 2000], and/or dynamic uplift [*Moucha et al.*, 2008, 2009; *Liu et al.*, 2010]. No consensus on the uplift contributed by each factor has yet been achieved. Knowledge of the present-day depth of the lithosphere-asthenosphere boundary (LAB) determined seismically from our Rayleigh wave tomography model can shed some light on the various uplift scenarios, given an assumed initial configuration. To better image the edge convective processes in the upper mantle and examine the feasibility of a regional delamination hypothesis [*Levander et al.*, 2011], we present a new Vs model based on a two-step inversion of Rayleigh wave data using the USArray data. This 3-D model provides absolute shear velocities allowing us to identify possible zones of partial melt at the CP edges, and produces the geometry of the lithosphere and asthenosphere for testing the delamination model at the western margin of the CP.

2. Data and Methodology

2.1. USArray Stations and Data Analysis

[6] The final Vs model provides crustal and upper mantle structures to ~200–250 km depth. We used phase and amplitude information of the fundamental mode Rayleigh waves recorded by the EarthScope/USArray Transportable Array (TA) network and several other seismic networks in the southwestern United States within the geographic boundaries 32° to 50°N latitude, and 116° to 105°W longitude. Data from about 200 broadband seismic stations in the TA network (station spacing ~70 km) and 18 stations in other networks were incorporated in the analysis, as shown in Figure 1. We have used a total of 154 teleseismic earthquakes ($30° \leq \Delta \leq 120°$, Figure 2a) with shallow focus (≤70 km) and magnitude ≥5.5 which occurred between June 2007 and September 2009, when the TA occupied the CP region. The good azimuthal distribution of events and well-distributed stations provide extremely dense raypath coverage (e.g., Figure 2b), allowing for good resolution of stable lateral fluctuations in phase velocities measured across the plateau region and its adjacent provinces.

[7] We processed the vertical components of the seismograms to extract the pure Rayleigh wave signals. After instrument response correction, we applied 18 Butterworth bandpass filters with 10 mHz bandwidth at center periods of 20, 22, 25, 27, 30, 34, 40, 45, 50, 59, 67, 77, 87, 100, 111, 125, 143, and 167s (50, 45, 40, 37, 33, 29, 25, 22, 20, 17, 15, 13, 11.5, 10, 9, 8, 7, and 6 mHz) to the preselected traces (see example in Figure 2c). The filtered seismograms with either unusual amplitudes or low signal-to-noise ratios (<3) were excluded; only highly coherent and clean traces were kept for analysis. To isolate the fundamental mode from higher-order modes and body wave phases, we windowed the surface waves with variable length tapered windows. The effects of frequency-dependent anelastic attenuation and geometrical spreading were taken into account for amplitude corrections [*Mitchell*, 1995; *Li et al.*, 2003]. Local site responses were also considered to account for individual station corrections of both amplitude amplification and phase shift [*Yang and Forsyth*, 2006a]. Earthquake magnitude variations

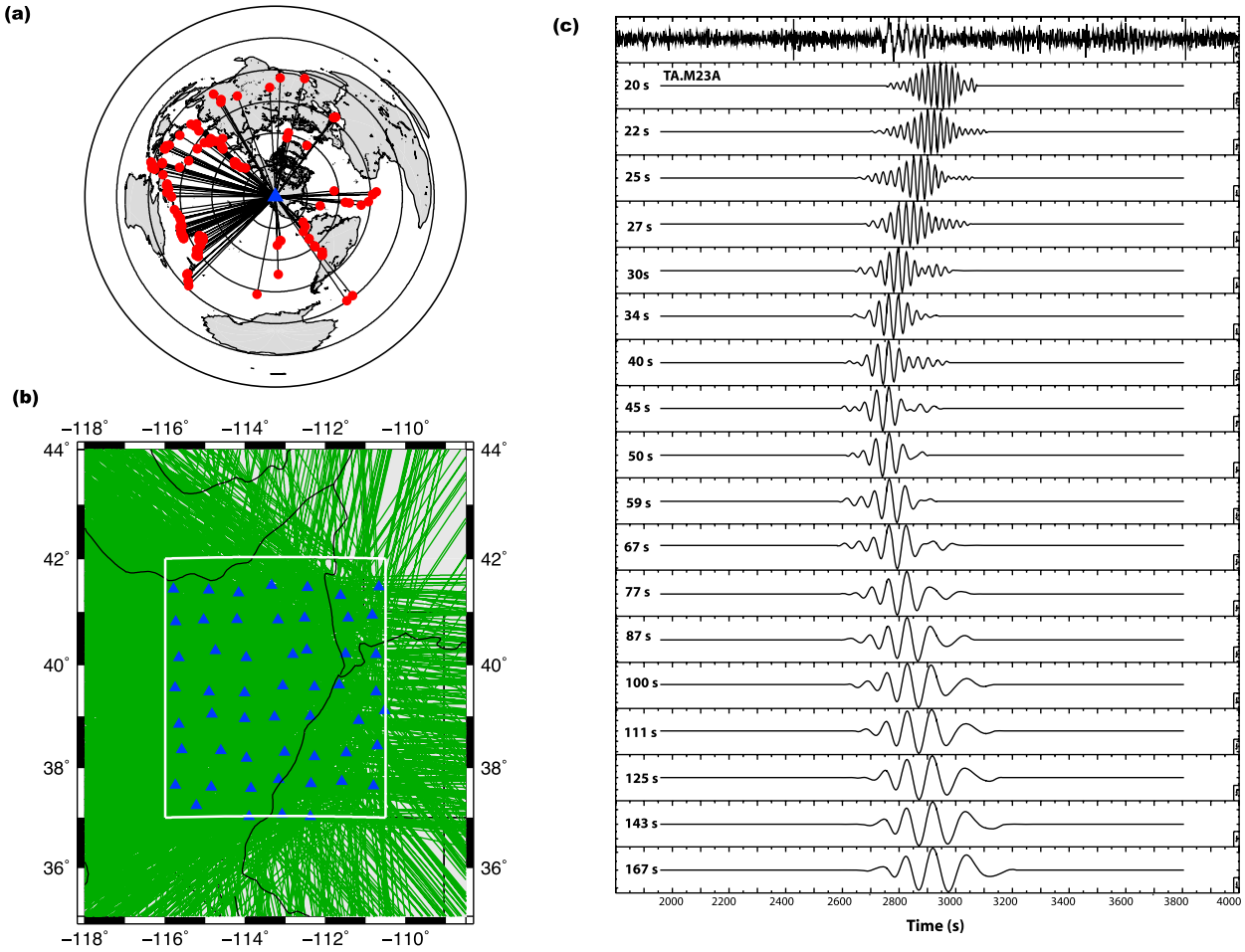

Figure 2. (a) Azimuthal distribution of earthquakes (red dots) used as the Rayleigh wave sources centered on the Colorado Plateau (blue triangle). The neighboring concentric circles are in 30° increments. (b) Raypath (green lines) coverage at 50 s for the Colorado Plateau-Northern Basin and Range subregion within the white box. Blue triangles represent the USArray stations. (c) An example of fundamental mode Rayleigh waveform at different frequency bands recorded at the M23A station in the USArray/TA network for an earthquake (magnitude 6.4, depth 35 km, and epicentral distance 98.3°) on 17 February 2009. The vertical component of the raw data is shown at the top and was filtered into18 frequency bands with central periods ranging from 20 to 167 s.

were removed by normalizing the observed amplitudes to the root mean square (RMS) amplitude for each event.

2.2. Finite Frequency Rayleigh Wave Tomography

[8] We have used the two-stage inversion developed by *Yang and Forsyth* [2006b] to determine the 3-D Vs structure from the phase and amplitude data. In the first step we obtain the 2-D phase velocities, with the modified two-plane wave technique [*Yang and Forsyth*, 2006a, 2006b; *Forsyth and Li*, 2005], effectively unraveling interference in the Rayleigh wavefield resulting from multipathing. The method assumes that at a given frequency, the complexity and distortion of the fundamental mode Rayleigh waves results from the sum of two interfering plane waves with different wave parameters (amplitudes, initial phases, angles of deviation from the great circle path). Additionally, we followed *Yang and Forsyth*'s [2006b] consideration of off-azimuth structures by introducing 2-D finite frequency amplitude and phase sensitivity kernels to resolve localized wavelength-scale heterogeneities. This method for determining phase velocities, with and without the finite frequency kernels, has been applied successfully to many data sets [*Forsyth et al.*, 1998; *Li et al.*, 2003, 2005; *Yang and Forsyth*,

2006a; *Yang and Ritzwoller*, 2008; *Schutt et al.*, 2008; *Miller et al.*, 2009].

[9] The inversion of phase velocity coefficients and wave parameters uses both simulated annealing and a generalized linearized inversion technique [*Forsyth and Li*, 2005; *Tarantola and Valette*, 1982]. In this scheme, the perturbations to the current phase velocity model and wavefield parameters are iteratively updated, until they meet the numerical criteria for the misfit of phase velocities. Next, we inverted the local dispersion curves for 1-D Vs structures using the DISPER80 code [*Saito*, 1988]. We used a similar iterative, linearized solution to the nonlinear least squares regional 1-D Vs inversion to construct a juxtaposed 3-D shear velocity model. The crustal thickness constraints are from receiver function estimates [*Miller and Levander*, 2009].

3. Parameterization and Inversion

3.1. Rayleigh Wave Phase Velocity Measurement

3.1.1. Parameterization

[10] Lateral variations in phase velocity can be highly resolved using the modified two-plane wave method. One basic assumption of the method is that the study region is small enough that the recorded waveforms can be represented as an interference pattern between two plane waves. We are examining a large area (11° × 10°); therefore we first divided it into four subregions (Figure 1): CP-NBR, CP-SRM, CP-SBR, and CP-RGR. This division takes advantage of the dynamic deployment status of the TA stations (the majority in the west before January 2008, and full coverage largely in the east after December 2008). The phase velocities in the overlapping regions were averaged after separate subdivision inversion. Different events were chosen for each "box" to maintain a good station coverage and similar azimuthal distribution (Figures 3a and 3b). A Gaussian averaging function with a smoothing length of 65 km was used in the relative traveltime calculation and to smooth the sensitivity kernels. There are six wave parameters (for each plane wave: amplitude, initial phase, and deviation angle) to represent each event. Each "box" is parameterized on an evenly distributed grid with a spacing of 0.5° in the receiver-covered region, and 1.0° on the boundary to absorb traveltime residuals of the waves not modeled well by the two-plane wave representation, a process accomplished by assigning larger a priori standard deviations to the peripheral nodes. The initial average phase velocities were estimated from the synthetic dispersion curve based on a modified version of the 1-D Tectonic North America (TNA) model from *Grand and Helmberger* [1984].

3.1.2. Inversion and Dispersion Curves

[11] The phase velocity variations from 20 to 167 s in each model "box" were derived. Fewer seismograms at short periods (e.g., <30 s) were kept because of strong distortion and incoherent interference patterns among stations due to localized multipathing, focusing, or defocusing effects, and at longer periods (T > 100 s) due to the decreasing Rayleigh wave energy. The mean phase RMS misfits (Figure 3c) are mainly below 3 s, indicating a good fit except at the longest periods (>143 s) that have larger uncertainties of phase measurements. In order to examine the validity of the two-plane wave approximation we examine one single event (30 September 2007) at 50 s period (Figures 3g and 3h), which shows the predicted phase and amplitude data fit the observations well. Moreover, for most filtered seismograms, the secondary/primary amplitude ratios are smaller than 0.4 (Figure 3d), and the deviation angles of the primary waves are within ±10 degrees of the great circle path (Figures 3e and 3f). The small amplitude ratios and path deviations indicate that the two-plane wave representation is reasonable.

[12] Several consistent phase velocity anomalies associated with the regional geological features are identified (Figure 4). We observe (1) a profound low-velocity area in the southern Rocky Mountains at short periods (<50 s) associated with a relatively low crustal shear velocity and a thick crust beneath the Colorado Rockies; (2) at periods less than 30 s a large low-velocity area covering the Colorado Mineral Belt to the east of the CP; (3) relatively high phase velocities beneath the SBR which decrease abruptly upon entering the CP-SBR transition region; (4) two long NE trending low-velocity belts along the CP-NBR and the Jemez lineament in the CP-RGR transition regions; (5) consistently high phase velocities in the CP interior compared to the surrounding tectonic margins; (6) at periods >45 s, the high velocity over the CP is continuous with the high phase velocity anomaly north of the CP, although it is variably reduced around its peripheries adjacent to the extended province to the west, south and east; and (7) high velocities in the SBR at short periods (e.g., 20–30 s, Figure 4) which result from the shallow Moho, as

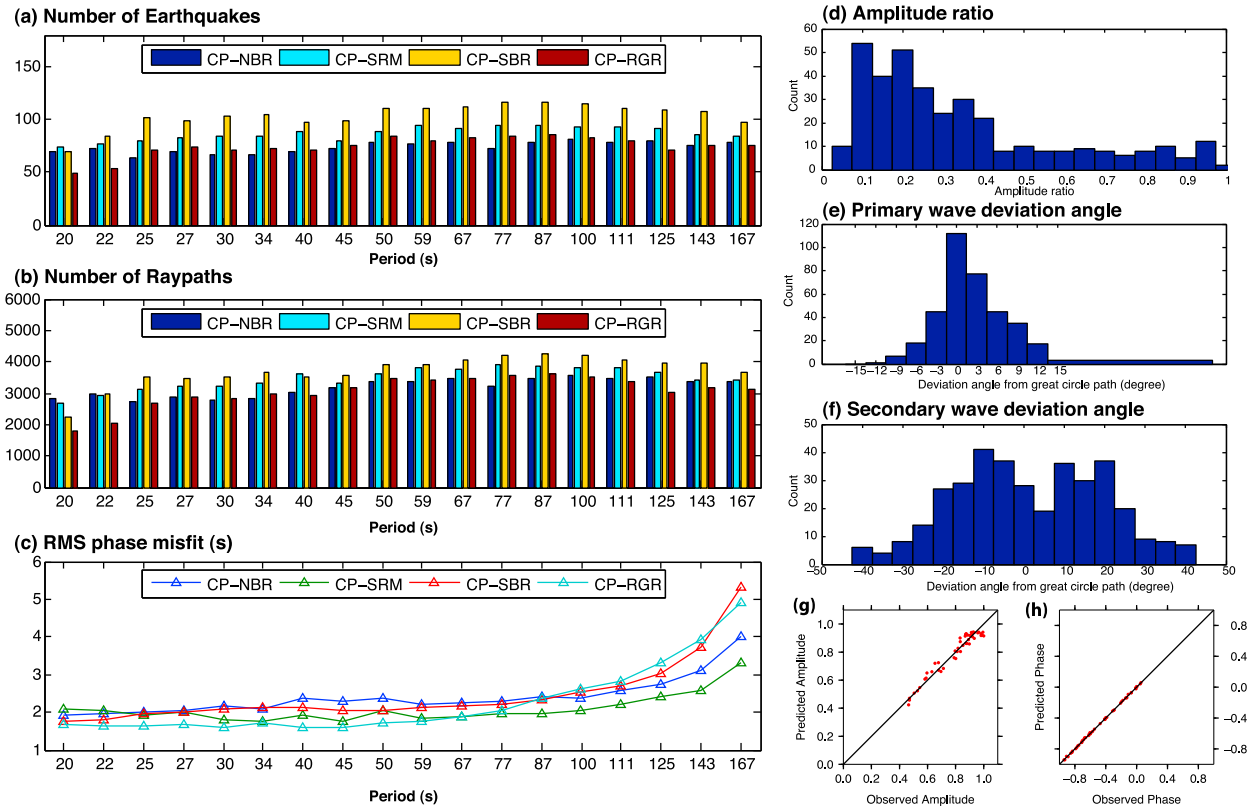

Figure 3. (a) Number of Rayleigh wave sources, (b) total number of raypaths, and (c) the phase RMS misfit in second for the phase velocity inversion at the 18 frequency bands at the four separate subregions: CP-NBR, CP-SRM, CP-SBR, and CP-RGR. Statistics of the inversion results of the two-plane wave approximation at 0.02 Hz (50 s) include (d) amplitude ratios of the smaller plane waves to the larger one, (e) deviation angles of the primary plane waves, and (f) deviation angles of the secondary plane waves from the great circle path. These angles are much larger than those of the primary waves. Comparison of predicted and measured (g) amplitude and (h) phase data at 50 s for the CP-NBR subregion.

Rayleigh waves in these periods sense upper mantle structures in the SBR, but the crust elsewhere.

3.2. Shear Velocity Inversion: Parameterization and Inversion

[13] The Rayleigh wave phase velocities have significantly greater sensitivity to the absolute shear velocity than to density and compressional velocity, especially below the Moho (Figure 5a). The vertical sensitivity kernels of Vp, Vs and density at various periods were computed based on the reference model, showing that the strongest sensitivity comes from the Vs profile. Thus, we kept density and Vp/Vs ratio fixed in each layer, and used a combined P and S wave sensitivity to calculate the perturbation to the previous velocity model. In practice, slightly varying the Vp/Vs ratio (1.70–1.85) caused no appreciable changes in the inversions. Thus, we finally used a fixed Vp/Vs ratio of 1.735 and 1.756 in the crust and upper mantle, respectively, the same as *Yang et al.* [2008] based on the statistical analysis of seismic parameters by *Chulick and Mooney* [2002]. The longest measured period (167 s) in the phase velocity indicates that the upper mantle structure can be well resolved as deep as ~250 km, though with larger vertical uncertainties.

[14] We iteratively inverted for shear velocity on the same 0.5° × 0.5° grid used for computing the Rayleigh wave dispersion curves. The average Vs structure was first inverted by taking a mean crustal thickness of 42 km based on the modified TNA model. Then we inverted for the localized Vs at each grid point using crustal thickness constraints from the RF study. The linearized inversion scheme uses a combination of minimum length and smoothing regularization by introducing nonzero diagonal and off-diagonal terms to the a priori

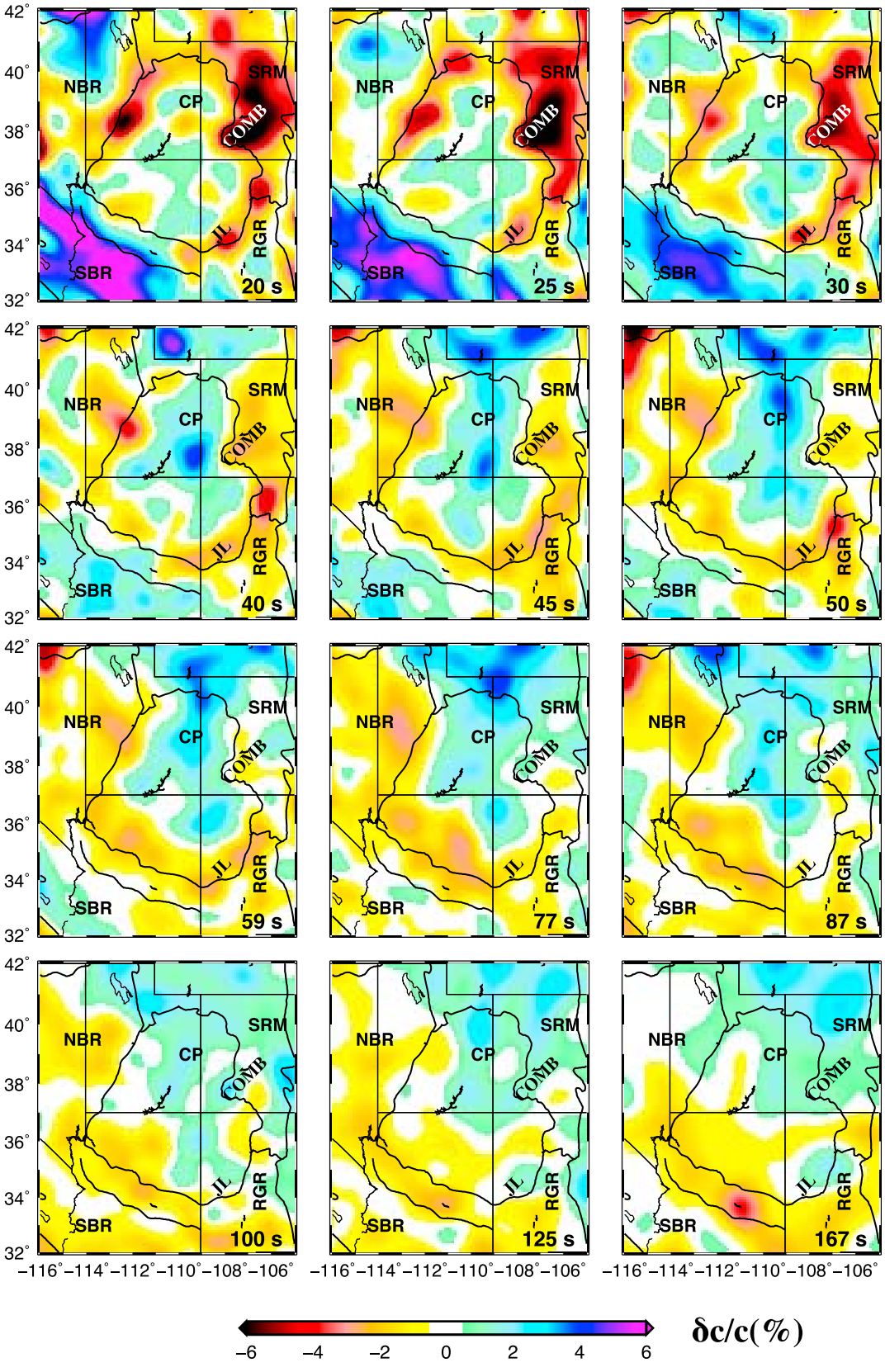

Figure 4. Rayleigh wave phase velocity maps at 12 of the 18 periods. The phase velocity inversions were performed separately on the four 0.5° × 0.5° grid subregions, created by cutting along two geographic lines at 110.5°W and 37°N, and were then combined by averaging the overlaps. COMB, Colorado Mineral Belt; JL, Jemez lineament.

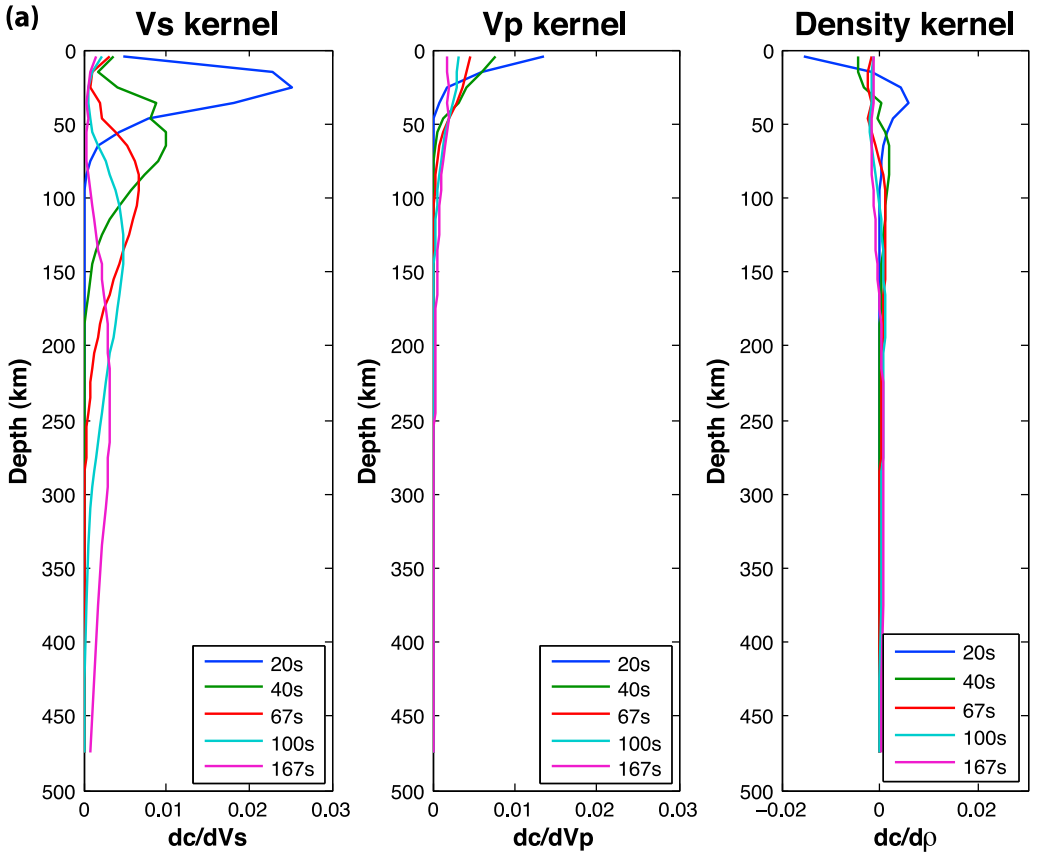
(a)
Vs kernel
Vp kernel
Density kernel
Depth (km)
dc/dVs
dc/dVp
dc/dρ
20s
40s
67s
100s
167s
(b) L curve
Damping Factor = 0.2
Model norm
Residue
(c) Rows of resolution matrix
Depth (km)
Resolution
15 km
55 km
105 km
155 km
205 km
310 km
425 km

Figure 5

model covariance matrix. A damping factor of 0.2 was suggested by the slope change in the L curve of the velocity model norm versus residuals of dispersion curves (Figure 5b), and agrees well with the choice of *Schutt et al.* [2008] by bounding the minimum upper mantle Vs to a reasonable range.

[15] The inversion of Vs structures can be evaluated from the resolution kernels at different depths. The resolution lengths for the reference model are plotted in Figure 5c, with the resolution peak displayed around 20 km for the row of the resolution matrix corresponding to 15 km. The number of adjacent layers needed to recover one entire piece of independent information of the model increases with depth, due to broader and weaker resolution peaks. The combined analysis from the Vs sensitivity and resolution kernels indicates that the S velocity can be well resolved to ~250 km depth, above which vertical and lateral heterogeneities are well imaged. The average Vs profiles beneath the entire region and the distinct tectonic regions are shown in Figure 6. We observe pronounced low-velocity zones beneath the SBR/NBR, the RGR and the SRM, which have been noted in many previous continental-scale studies [e.g., *Humphreys and Dueker*, 1994; *van der Lee and Nolet*, 1997; *Burdick et al.*, 2008].

4. Results

4.1. Crustal Heterogeneity

[16] The crustal structure in the study region is characterized by several multiscale (~50–100 km wide) high and low velocities (Figures 7a and 7b). Using the starting model (see section 3.2) as the reference, we have imaged several distinct low-velocity features surrounding the plateau, including two narrow transition regions (~50–100 km wide) from the Basin and Range, one beneath the Southern Rockies (Colorado Mineral Belt, Figures 7a and 7b), and one beneath the Jemez lineament near the Rio Grande Rift. The low crustal Vs anomalies (~150 km wide) beneath the CP-NBR transition region and the Colorado Rockies are broader than those in the CP-SBR transition region, and those beneath the Jemez lineament in the RGR-CP transition region (~100 km wide). The relatively high velocities (+3–4%) compared to the starting model under the SBR and NBR are separated by a low-velocity area located in the "magmatic gap" zone [e.g., *Armstrong and Ward*, 1991; *Zandt et al.*, 1995]. The high NBR velocities drop abruptly to the east of the Wasatch Front. In the Colorado Plateau interior, the crust is relatively complex and has an intermediate average velocity between the low-Vs RGR (Figures 7a and 7b) and the high-velocity Great Plains [e.g., *van der Lee and Nolet*, 1997; *West et al.*, 2004]. The NE trending high-velocity anomaly in the southern plateau is bounded by the Jemez lineament and the Yavapai/Southern Yavapai accretionary boundary (green dashed line in Figures 7a and 7b). It extends from the southeastern Navajo volcanic field region to the western edge of the SRM, and drops abruptly across the SRM-CP boundary into the Colorado Mineral Belt.

4.2. Upper Mantle Heterogeneity

[17] We also observe strong lateral velocity heterogeneity in the upper mantle relative to the TNA model (Figure 7). A large high-velocity feature (+1–3%) beneath 50–70% of the CP between 60 and 200 km depth extends from the Navajo volcanic field in the south across the NE striking Cheyenne Belt into the southern Archean Wyoming Province (Figures 7c–7h). Encircling this feature in the east, south and west are continuous, large amplitude (−2 to −6%) low velocities extending to ~125–150 km depth. The largest-amplitude low-velocity anomaly is located beneath the NBR to the west of the Wasatch Front (Figures 7c–7h). A NE trending narrow low-velocity belt (Figures 7f–7h) bisects the Four Corners high-velocity body.

[18] In the southeast, a "lambda-shaped" (λ) low-velocity body (green dashed contour in Figure 7c) is observed beneath the southern RGR and the Jemez volcanic fields (RGR/JL) (Figures 7c–7e). The two low-velocity trends of the "λ" merge close to the New Mexico-Colorado border, and extend northward into the SRM as Vs increases. The lowest shear velocity, ~8% lower than the global average, lies beneath the RGR axis where it crosses the Jemez lineament (Figures 7c–7e), in the depth range ~40 to 100 km. Below 100 km, the "λ" anomaly (Figures 7f and 7g) is lost to larger-scale

Figure 5. (a) Sensitivity kernel functions for S wave, P wave, and density at periods of 20, 40, 67, 100, and 167 s, based on the average shear velocity model. (b) Damping parameter estimation from the L curve of the Vs model norm and residuals of the phase velocity prediction. The turning point with damping parameter of 0.2 is chosen for the Vs inversion. (c) Model resolution kernels for layers at depths of 15, 55, 105, 155, 205, 310, and 425 km. Rows of the resolution matrix are calculated from the reference model.

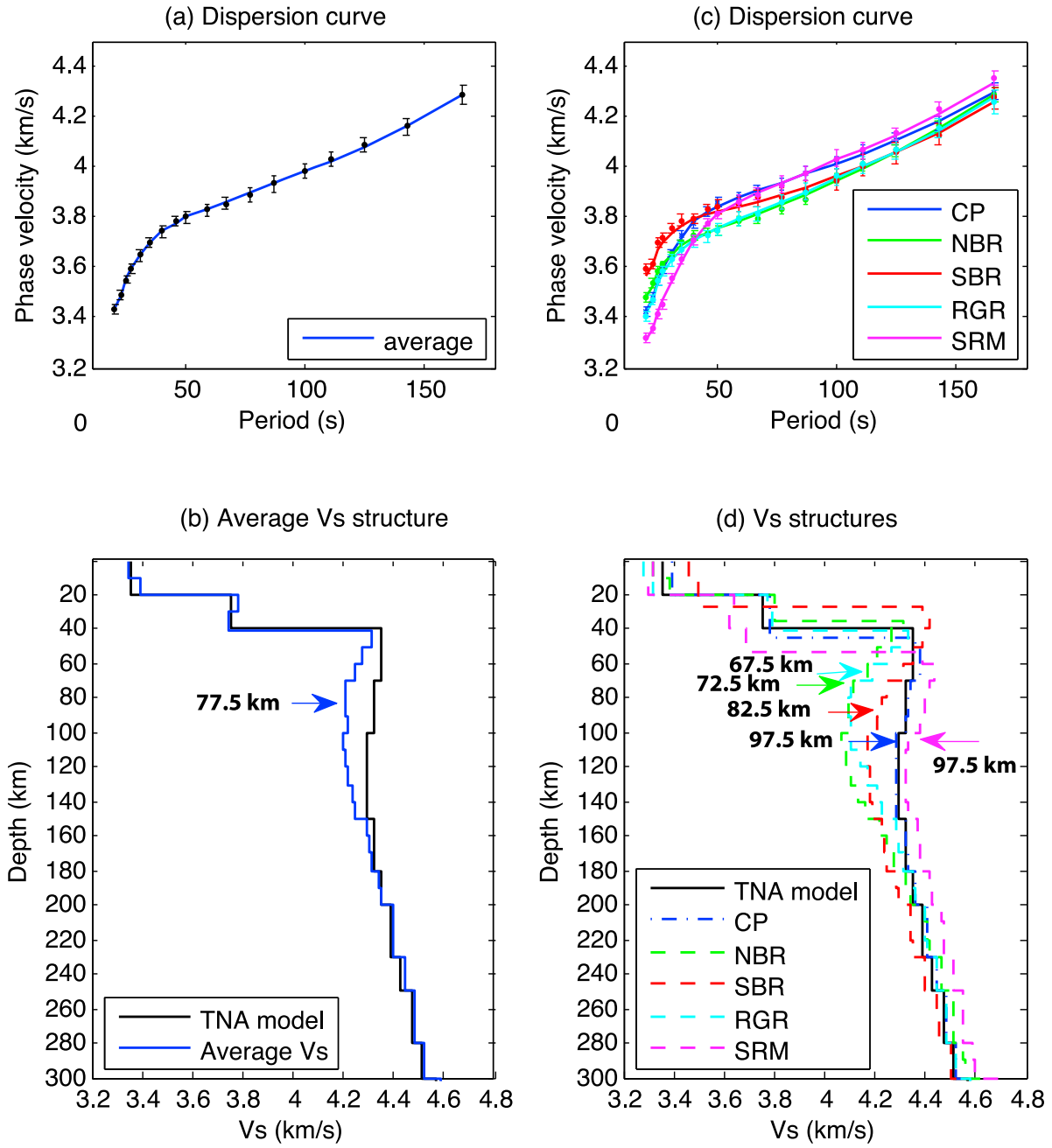

Figure 6. Dispersion curve fitting and Vs inversion. (a) The predicted dispersion curves for the average (blue) phase velocities. (b) The average Vs (blue) inverted from the starting modified TNA model (black) to fit the dispersion curve in Figure 6a. (c) The dispersion curves for five tectonic regions (CP, NBR, SBR, RGR, and SRM). (d) The average Vs models beneath the corresponding geologic regions. The colors are the same as in Figure 6c for each region, and the black line is the initial TNA model. All error bars represent the standard deviation of phase velocity measurements. Estimated LAB depths from the Rayleigh wave tomography at the center of the negative velocity gradients.

SBR low velocities. The velocity contrast between the Jemez lineament and the Four Corners high-velocity anomaly is large at ~10%. The low velocities in the RGR are bounded by higher velocities along the easternmost edge of the rift, where surface deformation in the western United States has largely ceased. At depths above 200 km (Figures 7c–7g), the upper mantle Vs peak-to-peak variations can reach as high as 12%. Weakening of the observed lateral heterogeneity at greater depths (>200 km, Figures 7h and 7i) is likely due to the loss of sensitivity and the lateral averaging effect of

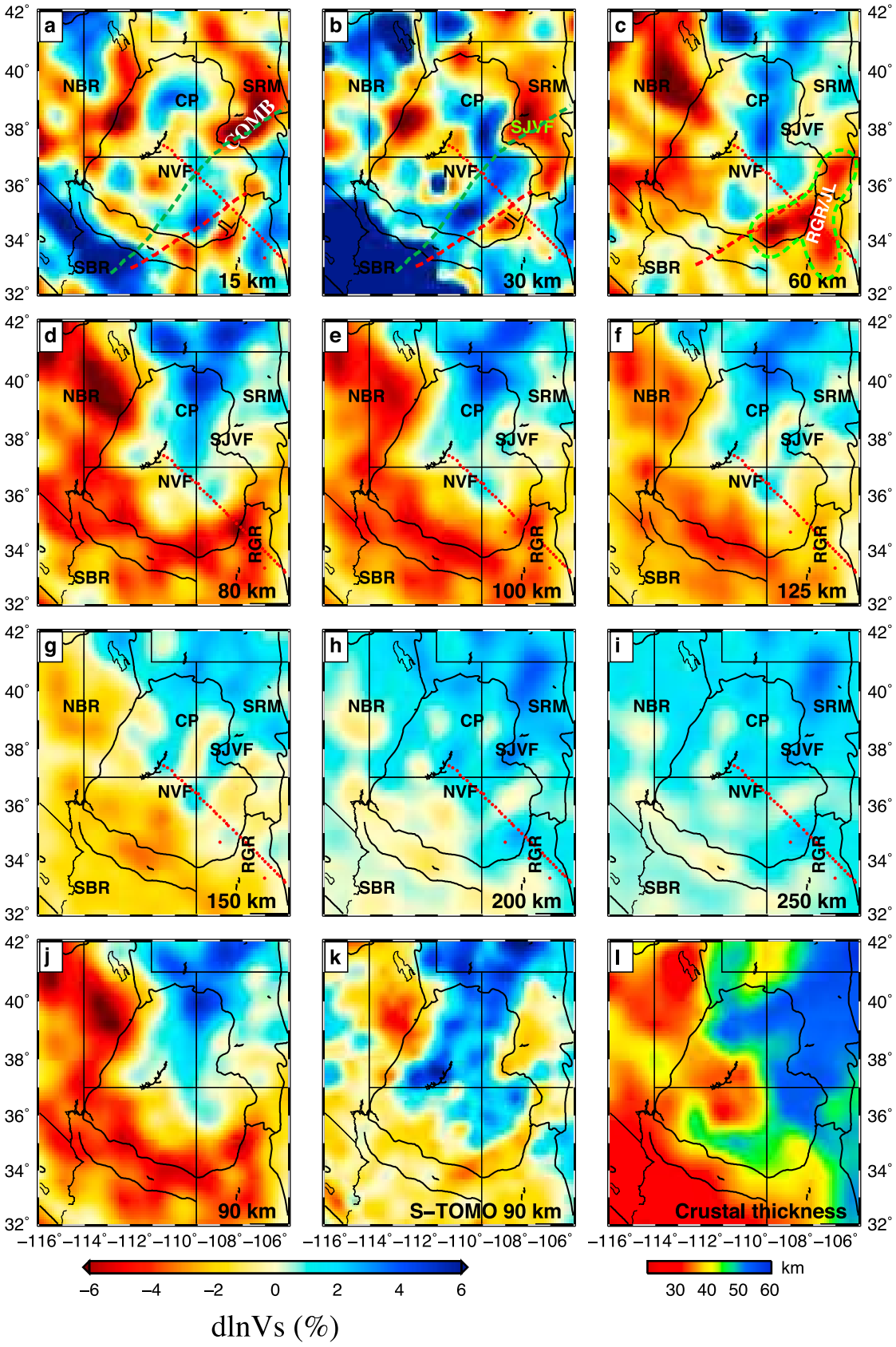
a
15 km
b
30 km
c
60 km
d
80 km
e
100 km
f
125 km
g
150 km
h
200 km
i
250 km
j
90 km
k
S–TOMO 90 km
l
Crustal thickness
NBR
CP
SRM
SJVF
NVF
SBR
RGR
COMB
42°
40°
38°
36°
34°
32°
–116°–114°–112°–110°–108°–106°
–6 –4 –2 0 2 4 6
dlnVs (%)
km
30 40 50 60

Figure 7

long-period Rayleigh waves, although it might also reflect the nature of the mantle heterogeneity at these depths.

4.3. LAB Depth Estimate

[19] The Rayleigh wave tomography model provides an independent estimate of the depth of the lithosphere-asthenosphere boundary (LAB) under and adjacent to the plateau. In a strict sense the LAB is a rheological boundary separating the conductive and rigid lithospheric lid from the convective and mechanically weak asthenosphere. Proxies for the LAB are often taken as geophysical discontinuities or vertical gradients in geophysical properties, negative in the case of seismic velocity, seismic impedance, or viscosity, and positive in the case of heat flow and electrical conductivities [*Eaton et al.*, 2009; *Fischer et al.*, 2010; *Abt et al.*, 2010]. The Ps and Sp RF techniques [e.g., *Langston* 1979; *Li et al.*, 2007] have been developed to detect such seismic impedance discontinuities effectively. However, the LAB depth is still sometimes ambiguously defined from RF images alone [*Rychert and Shearer*, 2009; *Yuan and Romanowicz*, 2010]. Additional constraint from the surface wave model, which is an estimate of absolute shear velocity, improves the determination of LAB depths. The LAB topography in the tectonically active southwestern United States is an important constraint for determining the geodynamic evolution of the BRP/RGR and the little-deformed CP, and for estimating the location of partial melts, which were probably generated and transported from greater depth in the upper mantle, and now reside under the young volcanic fields in the BRP and RGR regions. Detailed knowledge of the regional-scale mantle convection and thermal structures also depends significantly on the accuracy of the LAB topography.

[20] We obtained a new LAB map (Figure 9) by using the surface wave Vs model as a guide to pick the LAB depth from the Ps receiver function images. We first take the center of the negative upper mantle Vs gradient as the LAB depth [*Eaton et al.*, 2009; *Fischer et al.*, 2010], and compare it to the 3-D Ps and Sp RF volumes using the common conversion point (CCP) stacking technique [*Dueker and Sheehan*, 1997; *Levander et al.*, 2011; *Miller and Levander*, 2009]. There is good agreement between these two independent LAB depth estimates (Figure 8) though they are made from signals in different frequency bands (0.1–1.0 Hz for the RFs; 0.006–0.05 Hz in Rayleigh waves). For example in Figure 8, the LAB depth estimates at ~60–120 km from the RF images are, in most locations, well correlated with the top of the low velocities in the Vs images, in which selected RF profiles are plotted for direct comparison. The tomography Vs image reduces the ambiguity in choosing the LAB in Ps RFs where the negative converted Ps phase from the LAB is obscured by crustal multiple reflections. Due to the inherent smoothness of inverted gradients beneath the lithospheric high-velocity lid, using both surface wave inversion and receiver function images allows for distinction between multiple permissible LAB depth estimates. Thus, we finally picked the LAB depth from the receiver functions and the Vs profiles jointly.

[21] From the newly determined LAB map (Figure 9), we observe that the LAB beneath the BRP and RGR is relatively shallow at ~50–80 km depth. It is deeper beneath the CP at ~80–120 km, and becomes even deeper beneath the SRM to >150 km. The average LAB depths beneath each tectonic province show good agreement with depths inferred as the center of the negative-velocity gradient from the average Vs profiles (Figure 6). However, the relatively deep LAB (>85 km) of the plateau does not coincide with the physiographic province boundary: the abrupt lithospheric deepening beneath the CP lies within the plateau, not at the edges near the BRP/RGR (Figure 9).

5. Interpretation and Discussion

[22] The surface wave inversion results are consistent with numerous previous regional-scale or 2-D seismic studies such as PACE [e.g., *Wolf and Cipar*, 1993; *Benz and McCarthy*, 1994], Deep Probe [e.g., *Henstock et al.*, 1998; *Snelson et al.*,

Figure 7. Maps of Vs anomalies at depths of (a) 15, (b) 30, (c) 60, (d) 80, (e) 100, (f) 125, (g) 150, (h) 200, and (i) 250 km, relative to the TNA model, and comparison of (j) Vs maps at 90 km from this study and (k) the S body wave tomography [*Schmandt and Humphreys*, 2010]. Red and green dashed lines are the Yavapai/Southern Yavapai and Yavapai/Mazatzal accretionary boundaries, respectively. The "λ" anomaly in the upper mantle is shown as the light green dashed contour in Figure 7c. (l) The crustal thickness is estimated from the Ps receiver functions [*Miller and Levander*, 2009]. SJVF, San Juan volcanic fields; NVF, Navajo volcanic fields; COMB, Colorado Mineral Belt; JL, Jemez lineament. The red dotted line shows the station distribution of the La RISTRA experiment.

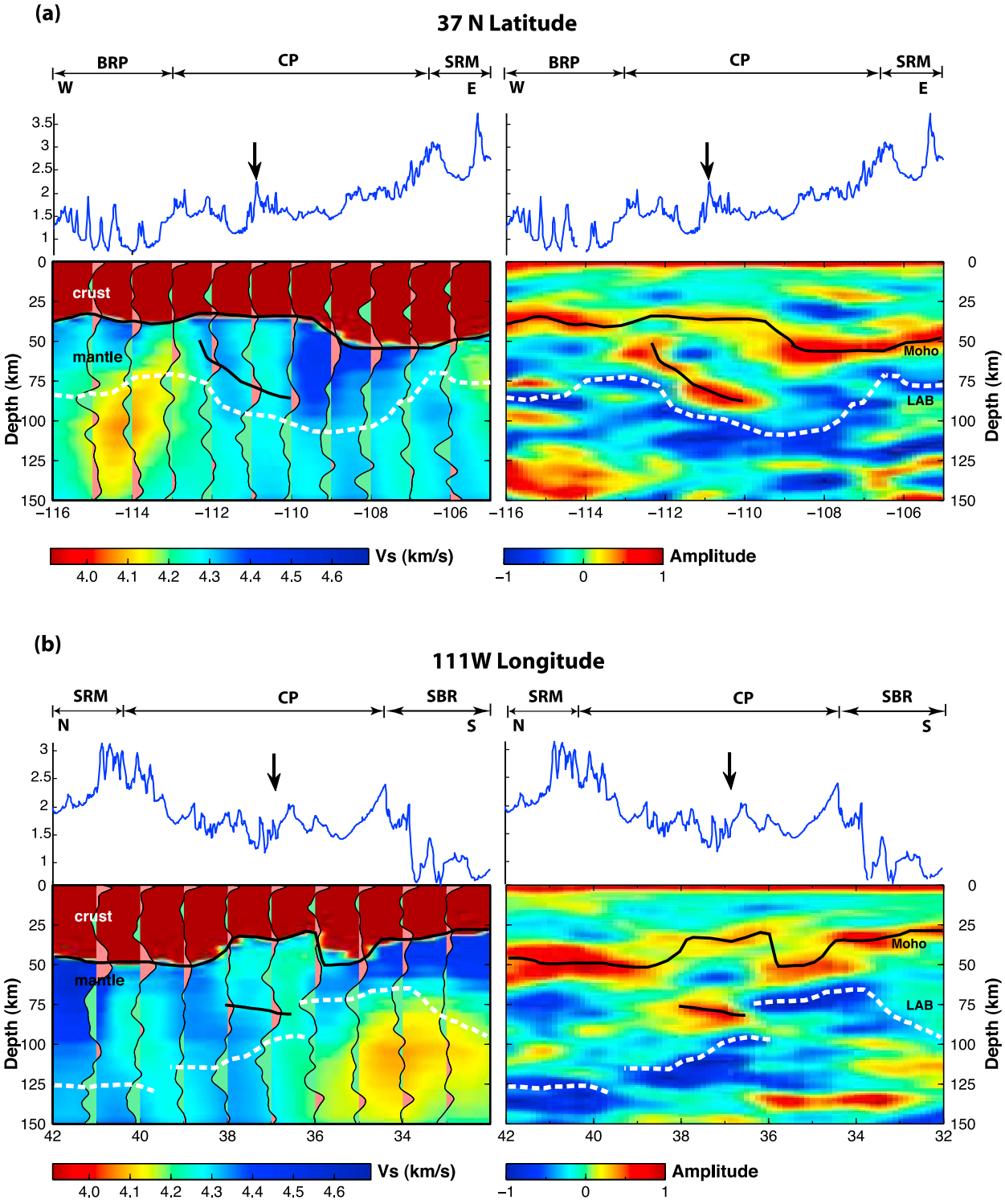

Figure 8. Comparison of cross sections of (left) shear velocity structure and (right) 1.25 Hz Ps receiver function images along (a) 37°N and (b) 111°W. The top of each image shows the elevation along the lines with arrows pointing at the Monument uplift (MU) where the delamination may start. The crustal velocity is set to a constant 3.9 km/s for display and plotted receiver function profiles (positive in light red and negative in light green) on the Vs cross sections. Black solid lines and white dashed ones indicate the Moho and LAB depths, respectively, estimated from the receiver functions.

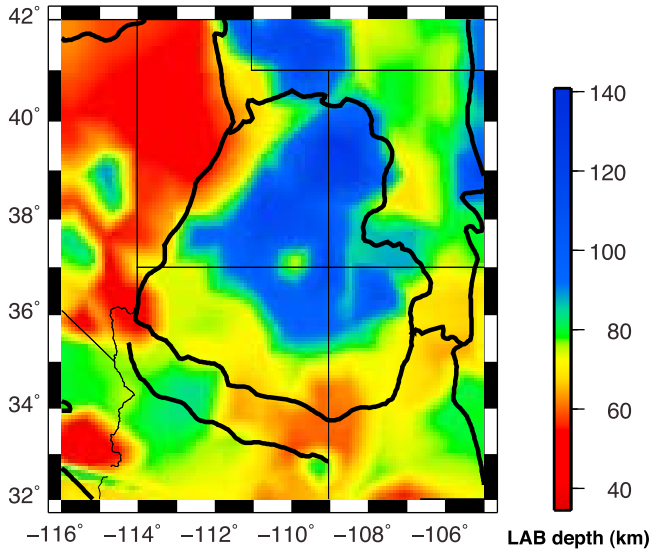

Figure 9. LAB depth map interpreted from the combined analysis from the receiver function and the Rayleigh wave tomography Vs volume.

1998], CD-ROM [e.g., *Levander et al.*, 2005; *Snelson et al.*, 2005], La RISTRA [e.g., *West et al.*, 2004; *Gao et al.*, 2004; *Wilson et al.*, 2005a, 2005b], and CP-GB [e.g., *Sheehan et al.*, 1995, 1997]. In addition, our model provides a 3-D examination of the complicated CP lithospheric structures over a wider region. The complicated lateral heterogeneity of the crustal and upper mantle Vs structures above 80 km can be attributed to Cenozoic magmatic modifications and tectonism around the plateau periphery, such as melt generation during the magmatic encroachment toward the CP center [*Roy et al.*, 2009], the possible warming from the extension around the margins, and the small rotation of the plateau [e.g., *Aldrich et al.*, 1986]. The thin BRP and RGR lithosphere result from Cenozoic extension, while the relatively thick central CP lithosphere is consistent with geologic observations that the plateau has experienced little internal deformation [*Thompson and Zoback*, 1979; *Morgan and Swanberg*, 1985]. Our results are in good agreement with the P and S body wave traveltime tomography results from *Schmandt and Humphreys* [2010], but have greater vertical resolution at shallow depths (<200 km). For example, comparing the Vs map at 90 km (Figures 7j and 7k), there appears to be similar lateral variation patterns with a large and continuous low-velocity anomaly surrounding the Four Corner high velocities from both methods. The slightly different magnitudes of anomalies can be attributed to radial anisotropy caused by continental deformation [*Moschetti et al.*, 2010]. Despite the larger station spacing of TA stations (~70 km), a cross section through our Vs volume shows similar high- and low-velocity anomalies as the more densely spaced (~20 km) La RISTRA experiment cross section [*Sine et al.*, 2008].

[23] Moreover, the surface wave model provides absolute Vs information rather than velocity perturbations derived from teleseismic body wave tomography [e.g., *Schmandt and Humphreys*, 2010; *Sine et al.*, 2008]. For instance, absolute velocity models can provide accurate traveltime computation, while, in contrast, the body wave tomography may give a biased result if using an incorrect reference model. Specifically, the absolute Vs can better constrain the upper mantle physical state in the Southwestern United States. For example, the lowest seismic velocities seen in Figure 11 are strongly correlated with locations of Late Cenozoic magmatism and high surface heat flow. We suggest that thermochemical convection occurs progressively inward into the plateau, removing the rehydrated and weakened parts of the CP lithosphere, and this convective process leads to magmatic migration inboard and produces a thinned lithospheric thickness and a low-velocity zone across the edge. At the western margin, a regional lithospheric downwelling process has been suggested by our surface waves, body wave tomography, and receiver functions [*Levander et al.*, 2011], and illustrates ongoing thermochemical convection involving the lowermost crust and upper mantle. This type of downwelling can help to explain how lithospheric mantle has been removed

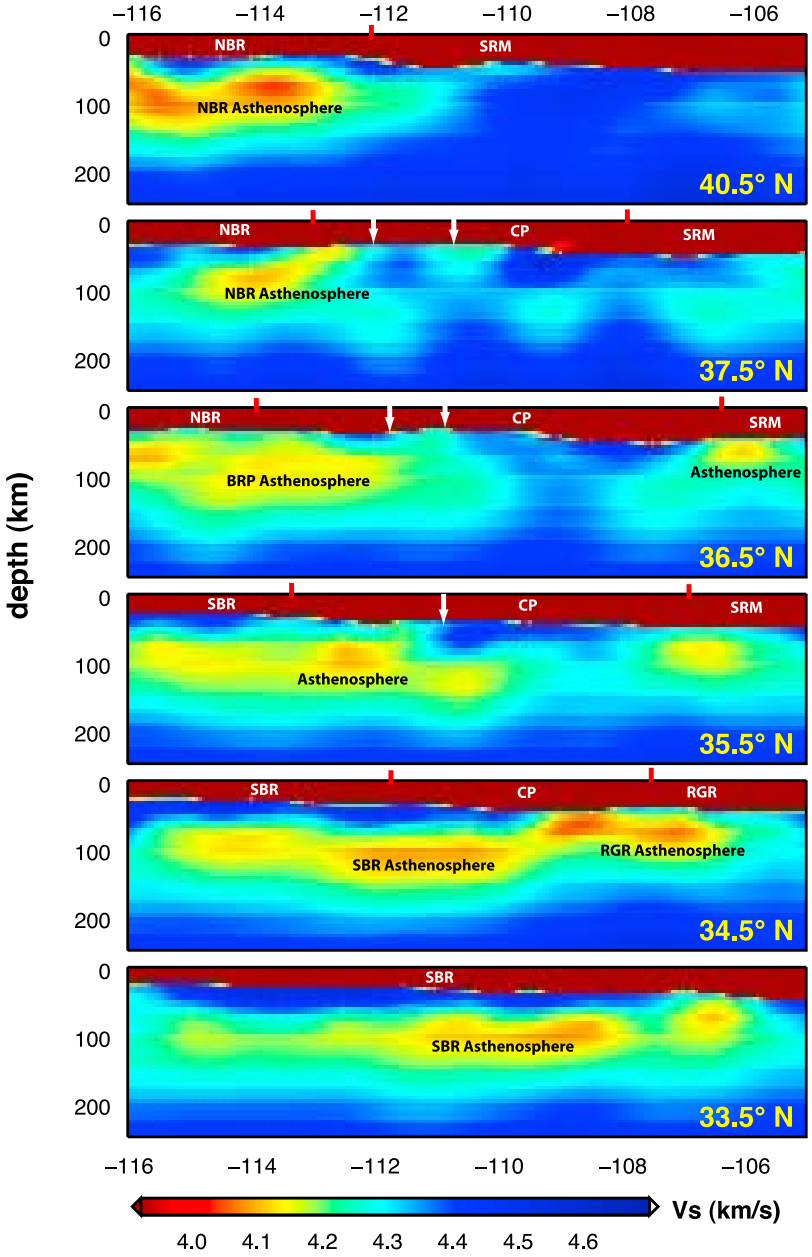

Figure 10. Vs cross sections along east-west traverses (labeled at the bottom right of each cross section) showing location of low-velocity zones, with tectonic boundaries marked as red ticks and suggested delamination location marked as white arrows.

around the CP, and how the crust in the CP-BR transition regions is thinned.

5.1. Upper Mantle Low Velocities

[24] In addition to the top of the low-velocity zone (LVZ) that we interpreted as the LAB, the base of the upper mantle LVZ can also be estimated from the tomographic images, although with larger uncertainties due to loss of vertical resolution at greater depths [*Eaton et al.*, 2009]. From the Vs cross sections (33.5°–40.5°N) in Figure 10, we observe that the LVZ shape changes significantly beneath different tectonic provinces. The LVZs beneath both the northern and southern BRP are very shallow (top at ~55–70 km) and thin (~90–120 km thick), and reach extremely low values (Vs < 4.15 km/s) at ~80–100 km depth under the transition region at the CP edge. The RGR/JL system has a shallower LAB (~50 km), a thinner LVZ (~70–90 km thick), and the minimum Vs (<4.0 km/s) at shallower depths of ~60–70 km. The

southernmost SRM has a low-velocity region at a similar depth as the RGR/JL system, but the absolute value of the lowest velocity increases northward by ~2–5%. There is no obvious well-defined low-velocity zone beneath the northern part of the plateau interior, although the LAB depth can still be roughly estimated from the small negative gradient in the Vs profiles. The penetration distances of the low-velocity zones (SBR: ~100–150 km; NBR: ~50–100 km), which extend across the CP tectonic boundary into the lithospheric core, correlate well with the eroded CP lithosphere inferred from the LAB topography obtained in this study (Figure 9). Assuming that the magmatic encroachment started from the edge at ~20 Ma when Basin and Range extension initiated with a uniform rate, we obtained a lateral rate of 5–7.5 km/Ma and 2.5–5 km/Ma from the SBR and NBR sides, respectively, which agrees well with the migration rates of surface volcanism presented by *Roy et al.* [2009]: SBR ~6.3 km/Ma; NBR ~4.0 km/Ma.

[25] Seismic velocity reduction is typically ascribed to changes in temperature [e.g., *Karato*, 1993; *Cammarano et al.*, 2003], volatile composition [e.g., *Karato and Jung*, 1998], degree of partial melt and melt depletion [e.g., *Hammond and Humphreys*, 2000; *Schutt and Lesher*, 2006], as well as seismic anisotropy [e.g., *Yang and Forsyth*, 2008] and grain size [e.g., *Faul and Jackson*, 2005]. The extremely strong Vs contrast (~12–14%) across ~80–125 km in the transition regions (Figures 7d–7f) cannot be simply caused by temperature variations, which require a physically unreasonable difference of ~600–900 K, if we used a temperature derivative $\delta \ln Vs/\delta T$ of ~1.5–2.3%/100 K [*Karato*, 1993; *Cammarano et al.*, 2003] and upper mantle attenuation Qs of ~50–100 [*Faul and Jackson*, 2005; *Sine et al.*, 2008; *Yang and Forsyth*, 2008; *Dalton et al.*, 2008]. The presence of a small amount of partial melt in the upper mantle LVZ can dramatically reduce the shear velocity and thus requires more reasonable temperature variation. *Hammond and Humphreys* [2000] suggested that a ~1% melt fraction in the upper mantle could cause at least a 7.9% reduction in shear velocity. If we assume ~1% partial melt in the low-velocity ring (Figure 11), the remaining Vs reduction can be caused by a lateral temperature variation of ~170–400 K, consistent with the 200–400 K temperature change suggested from xenolith data [*Riter and Smith*, 1996]. The required percentage of melt might be higher if we use the measurement by *Takei* [2000], which gives ~2–4% variations in Vs caused by 1% partial melt in the upper mantle. Compositional variations caused by hydration or melt depletion could also contribute a certain percentage to Vs reduction, but the contribution is too small to account for the observed Vs variations. Typically, no more than 0.5% change in Vs can be caused by the melt depletion in the upper mantle [*Schutt and Lesher*, 2006]. We interpret the upper mantle low velocities as resulting from a ~1% partial melt fraction in the lowest-velocity regions of the BRP, RGR and the southern and western peripheries of the CP. This has been previously suggested by *Schmandt and Humphreys* [2010] from body wave tomography, in which they observed low Vp, Vs, and high Vp/Vs. The partial melt could either be partially molten lithosphere whose solidus was depressed by hydration, or asthenospheric mantle. Geochemical data (e.g., $^{143}Nd/^{144}Nd$ ratios from *Crow et al.* [2011]) suggest that the melt source around the plateau rim has an increasingly asthenospheric signature through time. The locations of the asthenospheric low-velocity zones containing partial melt are strongly correlated with the existence of Holocene volcanic fields, which include the Valles Caldera and Zuni Bandera fields in the Jemez lineament, the San Francisco and Uinkaret fields at the southwestern edge, and the Markagunt Plateau and Bald Knoll, Santa Clara, and Black Rock Desert fields in the northwestern margin of the plateau (Figure 11).

5.2. Edge Convection Around the Colorado Plateau

[26] The 3-D scenario of edge convective erosion occurring around the CP boundary could be either an extension of 2-D edge driven thermal convection suggested by *van Wijk et al.* [2010], or numerous consecutive 3-D thermochemical convective events removing the lower crust and mantle lithosphere proposed by *Levander et al.* [2011], or both. In the latter case, erosion occurs by repeated localized drips, in the former by sheet-like drips. From the present-day configuration of the asthenospheric LVZs abutting the relatively high-Vs lithospheric core of the CP, we suggest that widespread small-scale convection is occurring at more than half of CP margins from the RGR to BRP to explain the present-day thinned lithosphere, localized uplift and magmatism at the edges. The shallowing trend of the LAB and base of the LVZs toward the plateau center could be related to the increasingly asthenospheric components observed toward the center of the plateau due to mantle upwelling [*Sine et al.*, 2008; *Crow et al.*, 2011].

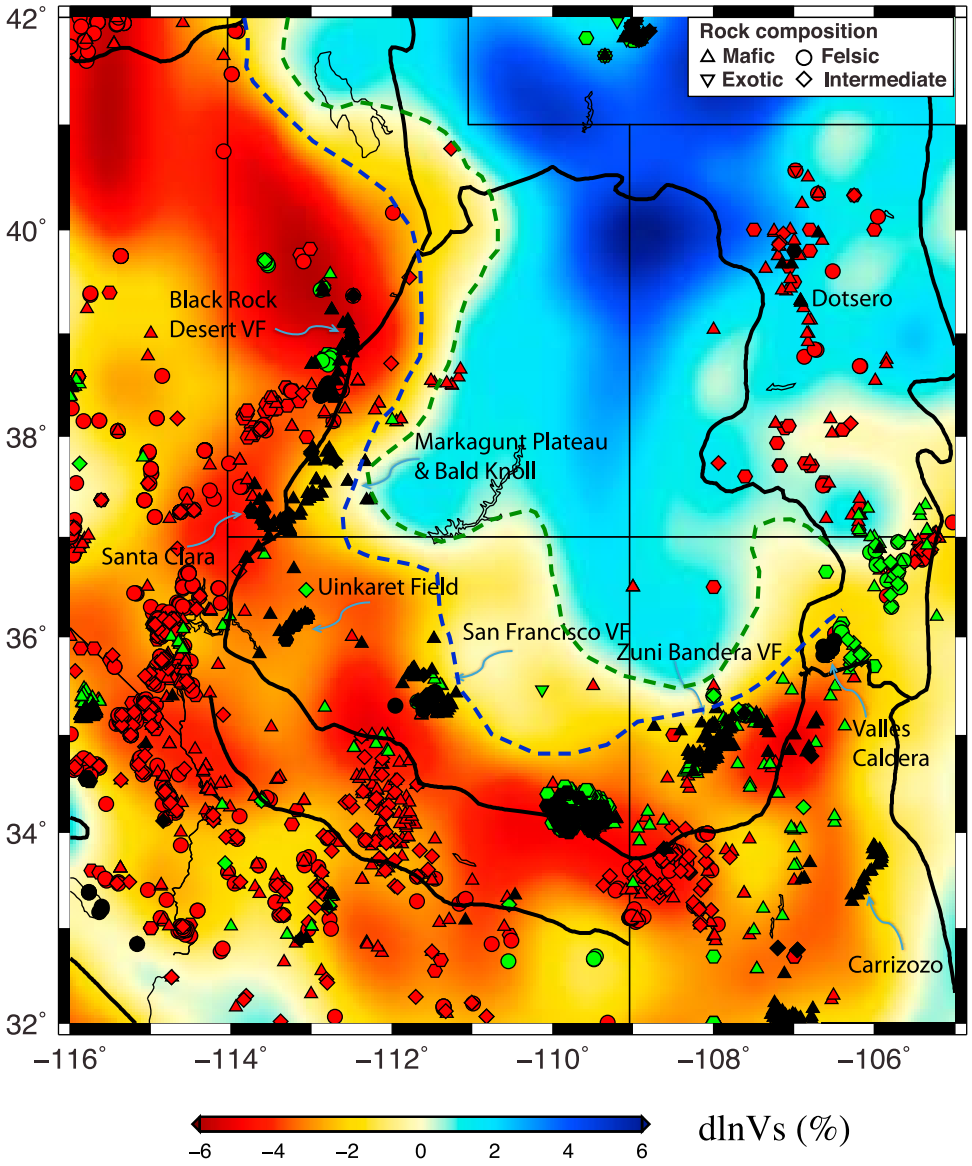

Figure 11. Rayleigh wave tomography Vs perturbation relative to TNA at 90 km depth. The types of the igneous volcanic rock compositions are plotted as different symbols as shown in the top right corner (data from NAVDAT: Western North American Volcanic and Intrusive Rock Database). The age of the rock is indicated by the fill color, where red means Miocene (23.7–5.3 Ma), green means Pliocene (5.3–1.8 Ma), and black means Quaternary (<1.8 Ma). The major Holocene volcanic fields are located at the CP edges, including Black Rock Desert volcanic field (VF), Markagunt Plateau and Bald Knoll, Santa Clara, Uinkaret field, San Francisco VF, Zuni Bandera VF, Valles Caldera, Dotsero, and Carrizozo. The blue dashed line is the contour of the low-velocity boundary coinciding well with the young magmatism, and the green dashed contour shows the high-velocity Proterozoic lithosphere.

[27] Widespread edge convection was probably developed initially from the large variations in lithospheric thickness (Figure 9) between the mildly deformed CP and the extended and thinned BRP and RGR since mid-Cenozoic, resulting in convective erosion of the CP thermal boundary layer as suggested by *van Wijk et al.* [2010] to explain the large Vs gradient and the magmatic invasion. Furthermore, we suggest that pervasive convective removal of both the thermal boundary layer and lithospheric core of the plateau has been progressively occurring across large parts of the periphery toward the northeastern cratonic root. The 3-D scenario of marginal erosion initiated from the large step of lithospheric thickness could be facilitated by rehydration and destabilization of CP lithosphere [*Humphreys et al.*, 2003; *Li et al.*, 2008]. Edge-driven convection itself cannot dra-

matically erode the abutting lithosphere without introducing substantial weakness inside the lithospheric root [*King and Anderson*, 1998]. Mantle xenolith evidence shows that the cold CP lithosphere, despite its depletion and little internal deformation, was rehydrated by subduction-released water and was further refertilized and mechanically weakened [*Li et al.*, 2008; *Roy et al.*, 2009]. The CP lithosphere, with significantly reduced viscosity at its base and flanks, is being convectively removed at a similar rate as the volcanic migration toward the CP interior although the process may be more three-dimensional than two-dimensional as suggested by the delamination-style downwelling under the Grand Canyon [*Levander et al.*, 2011].

[28] Our Vs model suggests that subcontinental convective processes might continue to erode and recycle the entire hydrated and destabilized lithosphere, and we predict coreward migration of low-velocity zones and thinned lithosphere. The convective erosion of the previously hydrated CP lithospheric core and the replacement by the lower-density asthenosphere contribute additional buoyancy at the western and southeastern edges. The uplift of the CP margins could further be facilitated by the thermal expansion from basal and side heating [*Roy et al.*, 2009]. Combining our new upper mantle Vs model and the geochemical analysis from *Crow et al.* [2011], we suggest that much of the low-velocity volume surrounding the plateau is associated with asthenospheric replacement of the CP lithosphere stripped off by convective erosion across the margins at various depths from the base of the crust to ~150 km.

5.3. Lithospheric Delamination and CP Uplift

[29] Cross sections of the Vs model support the ongoing regional delamination hypothesis in the western CP, as suggested by receiver functions, body wave tomography and our Rayleigh wave results [*Levander et al.*, 2011]. The CCP stacked RF images reveal unusually complicated Moho topography beneath the western portion of the plateau, where the conversion signals broaden and separate into two distinct positive-amplitude events (Figure 8). The top event is relatively shallow and is interpreted as a newly formed "elevated" Moho. The deeper one extends to depths of 70–90 km and is interpreted as the upper interface of a delamination-style, convective downwelling that includes the lower crust and upper mantle lithosphere [*Bird*, 1979; *Levander et al.*, 2011]. This feature appears in the teleseismic body wave tomography [*Schmandt and Humphreys*, 2010] as a high-velocity pipe extending to 200–250 km depth. In both seismic data sets, the feature is centered at about 37°N latitude and 111°W longitude, with a radius of ~100 km.

[30] At this point, the Rayleigh wave tomography shows high velocities that start at ~80 km depth and extend to the northeast to at least 100 km. Figure 8 shows a comparison of two cross sections from the RF and Rayleigh wave studies. The crustal thickness constraint in the Rayleigh wave phase velocity inversions is from the RF estimates as we describe below. To the west of the Navajo volcanic field (113–111°W in Figure 8a), a relatively high-velocity anomaly is imaged as hanging to the western edge of the plateau. Along the N-S profile, we also observed a high-velocity anomaly about 100 km across in the Vs image, the top of which correlates well with the top of the delamination event shown as the deeper positive Ps conversion in the RF image. The detachment direction indicates that the delamination of the lower crust and lithosphere propagates from the plateau interior toward the western margins of the plateau. This is consistent with increasing uplift rates in the Grand Canyon from west to east inferred from the incision history [*Karlstrom et al.*, 2008; *Levander et al.*, 2011]. The low-velocity region (111–110°W) east of the lithospheric drip, interpreted as the buoyant asthenosphere, is replacing the delaminating lithospheric mantle and lower crust.

[31] To test the robustness of the high-velocity structure beneath the delamination region, we have inverted the Vs structures using three different crustal thickness constraints (shallow, constant at 40 km, and deep Moho) beneath the western plateau. The shallow and deep Moho depths correspond to the shallow and deep events in the RF image (see Figure 8a), respectively. As anticipated, the lower crust and uppermost mantle velocity structures are greatly affected by different Moho constraints. However, we consistently observe the northeasterly dipping high-velocity feature in all the three Vs inversions, surrounded by low velocities from both sides in the west of the Navajo volcanic field (Figure 12). The consistent pipe-like upper mantle structures discount the possibility of an artifact introduced by an incorrect crustal thickness constraint. The shallow Moho inversion is preferred in this study because the data from the top positive event in the RF analysis is more physically reasonable since it is above 50 km. Moreover, the shallow Moho model produces the smallest residuals (<0.5%) in the inversion at about

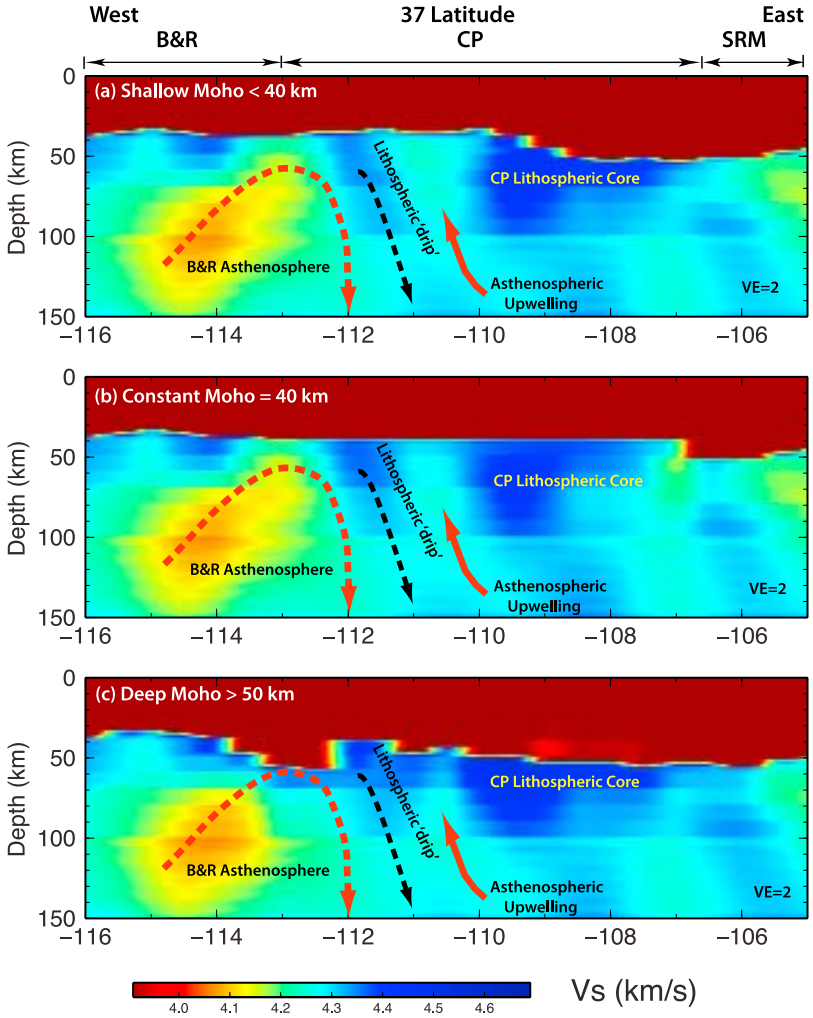

Figure 12. Three Vs cross sections along 37°N latitude from different inversion tests with constraints of crustal thickness beneath the delamination region: (a) shallow Moho (<40 km), (b) constant Moho (40 km), and (c) deep Moho (>50 km). The black dashed arrows show the convective downwelling drips of the lower crust and mantle lithosphere, which cause the asthenosphere to upwell to shallow depths (solid red arrow on the right). The dashed red arrows indicate the small-scale convective erosion at the edges. Vertical exaggeration (VE) is 2 for all the cross sections.

3–5 grid points over this region 36°–38°N, compared to the deep Moho model. The constant Moho model has similar residuals to the shallow model since their Moho depths are close.

[32] Our Vs model and inferred LAB topography, as well as the edge convection and regional downwelling, provide possible mechanisms for the complicated CP uplift observations at the margins. The crustal thickness from either active source data [*McCarthy and Parsons*, 1994; *Wolf and Cipar*, 1993; *Henstock et al.*, 1998; *Snelson et al.*, 1998] or Ps and Sp receiver functions [*Miller and Levander*, 2009] is inadequate to provide isostatic support for the ~1.8–2 km CP elevation. The preserved Proterozoic CP lithosphere, inferred from the high Vs in the core of the plateau and its thickness of ~100 km (Figures 6 and 9), makes the almost complete lithospheric removal following flat slab subduction [*Bird*, 1988] seem unlikely to us. Mantle compensation for the CP buoyancy is thus required; however, it cannot be fully explained by a single buoyancy source. Instead, we suggest several types of support that include dynamic uplift from a deep mantle upwelling [*Moucha et al.*, 2008, 2009; *Liu et al.*, 2010], basal/side heating and thermal expansion [*Thompson and Zoback*, 1979; *Roy et al.*, 2009], partial removal of lower crust and lithosphere components [*Spencer*, 1996; *Lastowka et al.*, 2001; *Levander et al.*, 2011], and small-

scale convective support along the CP margins [*van Wijk et al.*, 2008, 2010]. Though it is still difficult to quantify the buoyancy contribution from each mechanism [e.g., *Roy et al.*, 2009], our model suggests that both the edge convective asthenospheric source and the regional delamination can cause additional elevation at the western, southern, and southeastern margins of the plateau.

6. Conclusions

[33] We have developed a 3-D Vs model to ~250 km depth using USArray-based Rayleigh wave phase velocity data determined with finite frequency Rayleigh wave kernels and the two-plane wave method to separate multipathed arrivals. The resulting Vs model reveals strong lateral heterogeneity in the crust and uppermost mantle beneath the CP and the adjacent tectonic provinces. The Proterozoic CP lithosphere has high velocities relative to its peripheries and these high velocities extend to the north into the Rockies. A ring of low velocities in the upper mantle surround and extend under the CP periphery about ~100 km depth the CP-BRP transition region and the RGR/JL boundary. We interpret these low velocities as partially molten lithosphere or asthenosphere based on the geochemical signatures of volcanics in the region during the past 5–6 Myr. We suggest that the rehydrated and mechanically weakened CP lithosphere is progressively removed from the edges where low-velocity zones and thinned lithosphere are present, taking the form of either 2-D thermal or 3-D thermochemical convective erosion driven from the plateau edges by the thermal gradient and lithospheric thickness steps, and likely aided by asthenospheric melt invasion of the lithosphere. This edge convective process in 3-D and the complexity of the modern crustal and upper mantle structures under the plateau are understandable in terms of the lithospheric modification during the Cenozoic. By putting additional constraints from our Rayleigh wave Vs model with the Ps receiver function analysis, we have obtained a new LAB topography map. Our Vs model suggests that the lithosphere is removed at a rate similar to the magmatic encroachment toward the center of the plateau observed in surface volcanism. We note that the surface wave tomography provides additional seismic tomographic evidence for the delamination-style convective downwelling hypothesis in the western CP based on the RF imaging [*Levander et al.*, 2011]. A northeasterly dipping high-velocity anomaly, appearing regardless of the crustal thickness used in inversion, is interpreted as the convective downwelling of lower crust and mantle lithosphere at the western margin of the plateau. Based on previous studies and our new Vs model, we propose a hybrid uplift mechanism that includes a combination of chemical/thermal/geodynamic contributions, with buoyant support under the margins provided from lithospheric removal.

Acknowledgments

[34] The USArray seismic data were acquired from the IRIS DMC. We thank Donald Forsyth, Yingjie Yang, and Aibing Li for great help on the surface wave inversion code. We also thank Derek Schutt and another anonymous reviewer and the G^3 editor and associate editor for their constructive comments. We acknowledge Iain Bailey, Cin-Ty Lee, Adrian Lenardic, Tobias Höink, and Romain Bouchet for helpful discussion and thank Sally Thurner and Jen Gabler for editing the manuscript. B. Schmandt and E. Humphreys provided the body wave tomography model. Figures 1, 2, 4, and 7–12 were plotted using the GMT software [*Wessel and Smith*, 1998]. This research was supported by EarthScope NSF grants EAR-0844760 and EAR-0844741.

References

Abt, D. L., K. M. Fischer, S. W. French, H. A. Ford, H. Yuan, and B. Romanowicz (2010), North American lithospheric discontinuity structure imaged by *Ps* and *Sp* receiver functions, *J. Geophys. Res.*, *115*, B09301, doi:10.1029/2009JB006914.

Aldrich, M. J., Jr., C. E. Chapin, and A. W. Laughlin (1986), Stress history and tectonic development of the Rio Grande Rift, New Mexico, *J. Geophys. Res.*, *91*, 6199–6211, doi:10.1029/JB091iB06p06199.

Amante, C., and B. W. Eakins (2009), ETOPO1 1 arc-minute global relief model: Procedures, data sources and analysis, *NOAA Tech. Memo., NESDIS NGDC-24*.

Armstrong, R. L., and P. Ward (1991), Evolving geographic patterns of Cenozoic magmatism in the North American Cordillera: The temporal and spatial association of magmatism and metamorphic core complexes, *J. Geophys. Res.*, *96*, 13,201–13,224, doi:10.1029/91JB00412.

Benz, H. M., and J. McCarthy (1994), Evidence for an upper mantle low velocity zone beneath the southern Basin and Range-Colorado Plateau transition zone, *Geophys. Res. Lett.*, *21*, 509–512, doi:10.1029/93GL01660.

Bird, P. (1979), Continental delamination and the Colorado Plateau, *J. Geophys. Res.*, *84*, 7561–7571.

Bird, P. (1988), Formation of the Rocky Mountains, western United States: A continuum computer model, *Science*, *239*, 1501–1507, doi:10.1126/science.239.4847.1501.

Buehler, J. S., and P. M. Shearer (2010), Pn tomography of the western United States using USArray, *J. Geophys. Res.*, *115*, B09315, doi:10.1029/2009JB006874.

Burdick, S., C. Li, V. Martynov, T. Cox, J. Eakins, L. Astiz, F. L. Vernon, G. L. Pavlis, and R. D. van der Hilst (2008), Upper mantle heterogeneity beneath North America from travel time tomography with global and USArray transport-

able array data, *Seismol. Res. Lett.*, *79*(3), 384–392, doi:10.1785/gssrl.79.3.384.

Cammarano, F., S. Goes, P. Vacher, and D. Giardini (2003), Inferring upper mantle temperatures from seismic velocities, *Phys. Earth Planet. Inter.*, *138*, 197–222, doi:10.1016/S0031-9201(03)00156-0.

Chulick, G. S., and W. D. Mooney (2002), Seismic structure of the crust and uppermost mantle of North America and adjacent oceanic basins: A synthesis, *Bull. Seismol. Soc. Am.*, *92*(6), 2478–2492, doi:10.1785/0120010188.

Coney, P., and S. Reynolds (1977), Cordilleran benioff zones, *Nature*, *270*, 403–406, doi:10.1038/270403a0.

Crow, R., K. Karlstrom, Y. Asmerom, B. Schmandt, V. Polyak, and S. A. DuFrane (2011), Shrinking of the Colorado Plateau via lithospheric mantle erosion: Evidence from Nd and Sr isotopes and geochronology of Neogene basalts, *Geology*, *39*, 27–30, doi:10.1130/G31611.1.

Dalton, C. A., G. Ekström, and A. M. Dziewoński (2008), The global attenuation structure of the upper mantle, *J. Geophys. Res.*, *113*, B09303, doi:10.1029/2007JB005429.

Dickinson, W. R., and W. S. Snyder (1978), Plate tectonics of the Laramide Orogeny, in *Laramide Folding Associated With Basement Block Faulting in the Western United States*, edited by V. Matthews, *Mem. Geol. Soc. Am.*, *151*, 355–366.

Dueker, K. G., and A. F. Sheehan (1997), Mantle discontinuity structure from midpoint stacks of converted P to S waves across the Yellowstone hotspot track, *J. Geophys. Res.*, *102*, 8313–8327, doi:10.1029/96JB03857.

Eaton, D. W., F. Darbyshire, R. L. Evans, H. Grütter, A. G. Jones, and X. Yuan (2009), The elusive lithosphere-asthenosphere boundary (LAB) beneath cratons, *Lithos*, *109*(1–2), 1–22, doi:10.1016/j.lithos.2008.05.009.

English, J. M., S. T. Johnston, and K. L. Wang (2003), Thermal modeling of the Laramide orogeny: Testing the flat-slab subduction hypothesis, *Earth Planet. Sci. Lett.*, *214*, 619–632, doi:10.1016/S0012-821X(03)00399-6.

Faul, U. H., and I. Jackson (2005), The seismological signature of temperature and grain size variations in the upper mantle, *Earth Planet. Sci. Lett.*, *234*, 119–134, doi:10.1016/j.epsl.2005.02.008.

Fischer, K. M., H. A. Ford, D. L. Abt, and C. A. Rychert (2010), The lithosphere-asthenosphere boundary, *Annu. Rev. Earth Planet. Sci.*, *38*, 551–575, doi:10.1146/annurev-earth-040809-152438.

Forsyth, D. W., and A. Li (2005), Array analysis of two-dimensional variations in surface wave phase velocity and azimuthal anisotropy in the presence of multipathing interference, in *Seismic Earth: Array Analysis of Broadband Seismograms*, edited by A. Levander and G. Nolet, pp. 81–97, AGU, Washington, D. C.

Forsyth, D. W., S. Webb, L. Dorman, and Y. Shen (1998), Phase velocities of Rayleigh waves in the MELT experiment on the East Pacific Rise, *Science*, *280*, 1235–1238, doi:10.1126/science.280.5367.1235.

Gao, W., S. P. Grand, W. S. Baldridge, D. Wilson, M. West, J. F. Ni, and R. Aster (2004), Upper mantle convection beneath the central Rio Grande rift imaged by P and S wave tomography, *J. Geophys. Res.*, *109*, B03305, doi:10.1029/2003JB002743.

Gilbert, H. J., and A. F. Sheehan (2004), Images of crustal variations in the intermountain west, *J. Geophys. Res.*, *109*, B03306, doi:10.1029/2003JB002730.

Gilbert, H., A. A. Velasco, and G. Zandt (2007), Preservation of Proterozoic terrane boundaries within the Colorado Plateau and implications for its tectonic evolution, *Earth Planet. Sci. Lett.*, *258*(1–2), 237–248, doi:10.1016/j.epsl.2007.03.034.

Grand, S. P., and D. V. Helmberger (1984), Upper mantle shear structure of North America, *Geophys. J. R. Astron. Soc.*, *76*, 399–438.

Hammond, W. C., and E. D. Humphreys (2000), Upper mantle seismic wave velocity: Effects of realistic partial melt geometries, *J. Geophys. Res.*, *105*(B5), 10,975–10,986, doi:10.1029/2000JB900041.

Henstock, T., et al. (1998), Probing the Archean and Proterozoic lithosphere of western North America, *GSA Today*, *8*(7), 2–5.

Humphreys, E. D. (1995), Post-Laramide removal of the Farallon slab, western United States, *Geology*, *23*, 987–990, doi:10.1130/0091-7613(1995)023<0987:PLROTF>2.3.CO;2.

Humphreys, E. D. (2009), Relation of flat subduction to magmatism and deformation in the western United States, *Mem. Geol. Soc. Am.*, *204*, 85–98.

Humphreys, E. D., and K. G. Dueker (1994), Western U.S. upper mantle structure, *J. Geophys. Res.*, *99*, 9615–9634, doi:10.1029/93JB01724.

Humphreys, E., E. Hessler, K. Dueker, E. Erslev, G. L. Farmer, and T. Atwater (2003), How Laramide-age hydration of North America by the Farallon slab controlled subsequent activity in the Western U.S., *Int. Geol. Rev.*, *45*, 575–595, doi:10.2747/0020-6814.45.7.575.

Hyndman, R. D., C. A. Currie, and S. P. Mazzotti (2005), Subduction zone backarcs, mobile belts, and orogenic heat, *GSA Today*, *15*, 4–10.

Karato, S. (1993), Importance of anelasticity in the interpretation of seismic tomography, *Geophys. Res. Lett.*, *20*, 1623–1626, doi:10.1029/93GL01767.

Karato, S. I., and H. Jung (1998), Water, partial melting and the origin of the seismic low velocity and high attenuation zone in the upper mantle, *Earth Planet. Sci. Lett.*, *157*, 193–207, doi:10.1016/S0012-821X(98)00034-X.

Karlstrom, K. E., and G. Humphreys (1998), Influence of Proterozoic accretionary boundaries in the tectonic evolution of western North America: Interaction of cratonic grain and mantle modification events, *Rocky Mt. Geol.*, *33*(2), 161–179.

Karlstrom, K. E., R. Crow, L. J. Crossey, D. Coblentz, and J. van Wijk (2008), Model for tectonically driven incision of the less than 6 Ma Grand Canyon, *Geology*, *36*(11), 835–838, doi:10.1130/G25032A.1.

King, S. D., and D. L. Anderson (1998), Edge-driven convection, *Earth Planet. Sci. Lett.*, *160*, 289–296, doi:10.1016/S0012-821X(98)00089-2.

Langston, C. A. (1979), Structure under Mount Rainier, Washington, inferred from teleseismic body waves, *J. Geophys. Res.*, *84*, 4749–4762, doi:10.1029/JB084iB09p04749.

Lastowka, L. A., A. F. Sheehan, and J. M. Schneider (2001), Seismic evidence for partial delamination model for Colorado Plateau uplift, *Geophys. Res. Lett.*, *28*, 1319–1322, doi:10.1029/2000GL012360.

Lee, C.-T. A. (2005), Trace element evidence for hydrous metasomatism at the base of the North American lithosphere and possible association with Laramide low-angle subduction, *J. Geol.*, *113*, 673–685, doi:10.1086/449327.

Lee, C.-T., Q. Yin, R. L. Rudnick, and S. B. Jacobsen (2001), Preservation of ancient and fertile lithospheric mantle beneath the southwestern United States, *Nature*, *411*, 69–73, doi:10.1038/35075048.

Levander, A., C. A. Zelt, and M. B. Magnani (2005), Crust and upper mantle velocity structure of the Southern Rocky Mountains from the Jemez Lineament to the Cheyenne Belt, in *The Rocky Mountain Region: An Evolving Lithosphere*, *Geophys. Monogr. Ser.*, vol. 154, edited by K. Karlstrom and G. R. Keller, pp. 293–308, AGU, Washington, D. C.

Levander, A., B. Schmandt, M. S. Miller, K. Liu, K. E. Karlstrom, R. S. Crow, C.-T. A. Lee, and E. D. Humphreys (2011), Continuing Colorado plateau uplift by delamination-style convective lithospheric downwelling, *Nature*, *472*, 461–465, doi:10.1038/nature10001.

Li, A., D. W. Forsyth, and K. M. Fischer (2003), Shear velocity structure and azimuthal anisotropy beneath eastern North America from Rayleigh wave inversion, *J. Geophys. Res.*, *108*(B8), 2362, doi:10.1029/2002JB002259.

Li, A., D. W. Forsyth, and K. M. Fischer (2005), Rayleigh wave constraints on shear-wave structure and azimuthal anisotropy beneath the Colorado Rocky Mountains, in *The Rocky Mountain Region: An Evolving Lithosphere*, *Geophys. Monogr. Ser.*, vol. 154, edited by K. E. Karlstrom and G. R. Keller, pp. 385–401, AGU, Washington, D. C.

Li, X., X. Yuan, and R. Kind (2007), The lithosphere-asthenosphere boundary beneath the western United States, *Geophys. J. Int.*, *170*, 700–710, doi:10.1111/j.1365-246X.2007.03428.x.

Li, Z.-X. A., C.-T. A. Lee, A. H. Peslier, A. Lenardic, and S. J. Mackwell (2008), Water contents in mantle xenoliths from the Colorado Plateau and vicinity: Implications for the mantle rheology and hydration-induced thinning of continental lithosphere, *J. Geophys. Res.*, *113*, B09210, doi:10.1029/2007JB005540.

Lipman, P. W. (1992), Magmatism in the Cordilleran United States: Progress and problems, in *The Geology of North America*, vol. G3, *The Cordilleran Orogen, Conterminous U.S.*, edited by B. C. Burchfiel, P. W. Lipman, and M. L. Zoback, pp. 481–514, Geol. Soc. of Am., Boulder, Colo.

Liu, L., M. Gurnis, M. Seton, J. Saleeby, R. D. Muller, and J. Jackson (2010), The role of oceanic plateau subduction in the Laramide Orogeny, *Nat. Geosci.*, *3*, 353–357, doi:10.1038/ngeo829.

McCarthy, J., and T. Parsons (1994), Insights into the kinematic and Cenozoic evolution of the Basin and Range-Colorado Plateau transition from coincident seismic refraction and reflection data, *Geol. Soc. Am. Bull.*, *106*, 747–759, doi:10.1130/0016-7606(1994)106<0747:IITKCE>2.3.CO;2.

McCarthy, J., S. P. Larkin, G. S. Fuis, R. W. Simpson, and K. A. Howard (1991), Anatomy of a metamorphic core complex: Seismic refraction/wide-angle reflection profiling in southeastern California and western Arizona, *J. Geophys. Res.*, *96*(B7), 12,259–12,291, doi:10.1029/91JB01004.

McQuarrie, N., and C. G. Chase (2000), Raising the Colorado Plateau, *Geology*, *28*, 91–94, doi:10.1130/0091-7613(2000)028<0091:RTCP>2.0.CO;2.

Miller, M. S., and A. Levander (2009), Receiver function images of the western US lithosphere, *InSite Mag.*, summer, 2 pp., EarthScope Natl. Off., Corvallis, Oreg.

Miller, M. S., A. Levander, F. Niu, and A. Li (2009), Upper mantle structure beneath the Caribbean-South American plate boundary from surface wave tomography, *J. Geophys. Res.*, *114*, B01312, doi:10.1029/2007JB005507.

Mitchell, B. J. (1995), Anelastic structure and evolution of the continental crust and upper mantle from seismic surface wave attenuation, *Rev. Geophys.*, *33*, 441–462, doi:10.1029/95RG02074.

Morgan, P., and C. Swanberg (1985), On the Cenozoic uplift and tectonic stability of the Colorado Plateau, *J. Geodyn.*, *3*, 39–63, doi:10.1016/0264-3707(85)90021-3.

Morgan, P., W. R. Seager, and M. P. Golombek (1986), Cenozoic thermal, mechanical and tectonic evolution of the Rio Grande Rift, *J. Geophys. Res.*, *91*(B6), 6263–6276, doi:10.1029/JB091iB06p06263.

Moschetti, M. P., M. H. Ritzwoller, F. Lin, and Y. Yang (2010), Seismic evidence for widespread western-US deep-crustal deformation caused by extension, *Nature*, *464*, 885–889, doi:10.1038/nature08951.

Moucha, R., A. M. Forte, D. B. Rowley, J. X. Mitrovica, N. A. Simmons, and S. P. Grand (2008), Mantle convection and the recent evolution of the Colorado Plateau and the Rio Grande Rift valley, *Geology*, *36*, 439–442, doi:10.1130/G24577A.1.

Moucha, R., A. M. Forte, D. B. Rowley, J. X. Mitrovica, N. A. Simmons, and S. P. Grand (2009), Deep mantle forces and the uplift of the Colorado Plateau, *Geophys. Res. Lett.*, *36*, L19310, doi:10.1029/2009GL039778.

Parsons, T., J. McCarthy, W. M. Kohler, C. J. Ammon, H. M. Benz, J. A. Hole, and E. E. Criley (1996), Crustal structure of the Colorado Plateau, Arizona: Application of new long-offset seismic data analysis techniques, *J. Geophys. Res.*, *101*, 11,173–11,194, doi:10.1029/95JB03742.

Riter, J., and D. Smith (1996), Xenolith constraints on the thermal history of the mantle below the Colorado Plateau, *Geology*, *24*, 267–270, doi:10.1130/0091-7613(1996)024<0267:XCOTTH>2.3.CO;2.

Roy, M., T. H. Jordan, and J. L. Pederson (2009), Colorado Plateau magmatism and uplift by warming of heterogeneous lithosphere, *Nature*, *459*, 978–982, doi:10.1038/nature08052.

Rychert, C. A., and P. M. Shearer (2009), A global view of the lithosphere-asthenosphere boundary, *Science*, *324*, 495–498, doi:10.1126/science.1169754.

Saito, M. (1988), DISPER80: A subroutine package for the calculation of seismic normal-mode solutions, in *Seismological Algorithms, Computational Methods and Computer Programs*, pp. 293–319, Academic, New York.

Saleeby, J. (2003), Segmentation of the Laramide Slab—Evidence from the southern Sierra Nevada region, *Geol. Soc. Am. Bull.*, *115*, 655–668, doi:10.1130/0016-7606(2003)115<0655:SOTLSF>2.0.CO;2.

Schmandt, B., and E. Humphreys (2010), Complex subduction and small-scale convection revealed by body-wave tomography of the western United States upper mantle, *Earth Planet. Sci. Lett.*, *297*, 435–445, doi:10.1016/j.epsl.2010.06.047.

Schutt, D., and C. Lesher (2006), Effects of melt depletion on the density and seismic velocity of garnet and spinel lherzolite, *J. Geophys. Res.*, *111*, B05401, doi:10.1029/2003JB002950.

Schutt, D. L., K. Dueker, and H. Yuan (2008), Crust and upper mantle velocity structure of the Yellowstone hot spot and surroundings, *J. Geophys. Res.*, *113*, B03310, doi:10.1029/2007JB005109.

Sheehan, A. F., G. A. Abers, A. L. Lerner-Lam, and C. H. Jones (1995), Crustal thickness variations across the Colorado Rocky Mountains from teleseismic receiver functions, *J. Geophys. Res.*, *100*, 20,391–20,404, doi:10.1029/95JB01966.

Sheehan, A. F., C. H. Jones, M. K. Savage, S. Ozalabey, and J. M. Schneider (1997), Contrasting lithosphere structure between the Colorado Plateau and the Great Basin:

Initial results from Colorado Plateau-Great Basin PASSCAL experiment, *Geophys. Res. Lett.*, *24*, 2609–2612.

Sine, C. R., D. Wilson, W. Gao, S. P. Grand, R. Aster, J. Ni, and W. S. Baldridge (2008), Mantle structure beneath the western edge of the Colorado Plateau, *Geophys. Res. Lett.*, *35*, L10303, doi:10.1029/2008GL033391.

Snelson, C. M., T. J. Henstock, G. R. Keller, K. C. Miller, and A. Levander (1998), Crustal and uppermost mantle structure along the Deep Probe seismic profile, *Rocky Mt. Geol.*, *33*, 181–198.

Snelson, C. M., G. R. Keller, K. C. Miller, H.-M. Rumpel, and C. Prodehl (2005), Regional crustal structure derived from the CD-ROM 99 seismic refraction/wide-angle reflection profile: The lower crust and upper mantle, in *The Rocky Mountain Region—An Evolving Lithosphere: Tectonics, Geochemistry, and Geophysics*, *Geophys. Monogr. Ser.*, vol. 154, edited by K. E. Karlstrom and G. R. Keller, pp. 271–291, AGU, Washington, D. C.

Snyder, W. S., W. R. Dickinson, and M. L. Silberman (1976), Tectonic implications of space-time patterns of Cenozoic magmatism in the western United States, *Earth Planet. Sci. Lett.*, *32*, 91–106, doi:10.1016/0012-821X(76)90189-8.

Spencer, J. E. (1996), Uplift of the Colorado Plateau due to lithosphere attenuation during Laramide low-angle subduction, *J. Geophys. Res.*, *101*, 13,595–13,609, doi:10.1029/96JB00818.

Takei, Y. (2000), Acoustic properties of partially molten media studied on a simple binary system with a controllable dihedral angle, *J. Geophys. Res.*, *105*(B7), 16,665–16,682, doi:10.1029/2000JB900124.

Tarantola, A., and B. Valette (1982), Generalized non-linear problems solved using the least-squares criterion, *Rev. Geophys.*, *20*, 219–232, doi:10.1029/RG020i002p00219.

Thompson, G. A., and M. L. Zoback (1979), Regional geophysics of the Colorado Plateau, *Tectonophysics*, *61*, 149–181, doi:10.1016/0040-1951(79)90296-8.

van der Lee, S., and G. Nolet (1997), Upper mantle S-velocity structure of North America, *J. Geophys. Res.*, *102*, 22,815–22,838, doi:10.1029/97JB01168.

van Wijk, J., J. Van Hunen, and S. Goes (2008), Small-scale convection during continental rifting: Evidence from the Rio Grande rift, *Geology*, *36*, 575–578, doi:10.1130/G24691A.1.

van Wijk, J. W., W. S. Baldridge, J. van Hunen, S. Goes, R. Aster, D. D. Coblentz, S. P. Grand, and J. Ni (2010), Small-scale convection at the edge of the Colorado Plateau; implications for topography, magmatism, and evolution of Proterozoic lithosphere, *Geology*, *38*(7), 611–614, doi:10.1130/G31031.1.

Wessel, P., and W. H. F. Smith (1998), New, improved version of generic mapping tools released, *Eos Trans. AGU*, *79*(47), 579.

West, M., J. Ni, W. Baldridge, D. Wilson, R. Aster, W. Gao, and S. Grand (2004), Crust and upper mantle shear-wave structure of the southwest United States: Implications for rifting and support for high elevation, *J. Geophys. Res.*, *109*, B03309, doi:10.1029/2003JB002575.

Wilson, D., R. Aster, J. Ni, S. Grand, M. West, W. Gao, W. S. Baldridge, and S. Semken (2005a), Imaging the seismic structure of the crust and upper mantle beneath the Great Plains, Rio Grande Rift, and Colorado Plateau using receiver functions, *J. Geophys. Res.*, *110*, B05306, doi:10.1029/2004JB003492.

Wilson, D., R. Aster, M. West, J. Ni, S. Grand, W. Gao, W. Baldridge, S. Semken, and P. Patel (2005b), Lithospheric structure of the Rio Grande rift, *Nature*, *433*, 851–855, doi:10.1038/nature03297.

Wilson, D. C., R. Aster, S. Grand, J. Ni, and W. S. Baldridge (2010), High-resolution receiver function imaging reveals Colorado Plateau lithospheric architecture and mantle-supported topography, *Geophys. Res. Lett.*, *37*, L20313, doi:10.1029/2010GL044799.

Wolf, L. W., and J. J. Cipar (1993), Through thick and thin: A new model for the Colorado plateau from seismic refraction data from Pacific to Arizona crustal experiment, *J. Geophys. Res.*, *98*, 19,881–19,894, doi:10.1029/93JB02163.

Yang, Y., and D. W. Forsyth (2006a), Rayleigh wave phase velocities, small-scale convection, and azimuthal anisotropy beneath southern California, *J. Geophys. Res.*, *111*, B07306, doi:10.1029/2005JB004180.

Yang, Y., and D. W. Forsyth (2006b), Regional tomographic inversion of amplitude and phase of Rayleigh waves with 2-D sensitivity kernels, *Geophys. J. Int.*, *166*, 1148–1160, doi:10.1111/j.1365-246X.2006.02972.x.

Yang, Y., and D. W. Forsyth (2008), Attenuation in the upper mantle beneath Southern California: Physical state of the lithosphere and asthenosphere, *J. Geophys. Res.*, *113*, B03308, doi:10.1029/2007JB005118.

Yang, Y., and M. H. Ritzwoller (2008), Teleseismic surface wave tomography in the western U.S. using the Transportable Array component of USArray, *Geophys. Res. Lett.*, *35*, L04308, doi:10.1029/2007GL032278.

Yang, Y., M. H. Ritzwoller, F.-C. Lin, M. P. Moschetti, and N. M. Shapiro (2008), Structure of the crust and uppermost mantle beneath the western United States revealed by ambient noise and earthquake tomography, *J. Geophys. Res.*, *113*, B12310, doi:10.1029/2008JB005833.

Yuan, H., and B. Romanowicz (2010), Lithospheric layering in the North American continent, *Nature*, *466*, 1063–1068, doi:10.1038/nature09332.

Zandt, G., S. C. Myers, and T. C. Wallace (1995), Crust and mantle structure across the Basin and Range-Colorado Plateau boundary at 37°N latitude and implications for Cenozoic extensional mechanism, *J. Geophys. Res.*, *100*, 10,529–10,548, doi:10.1029/94JB03063.